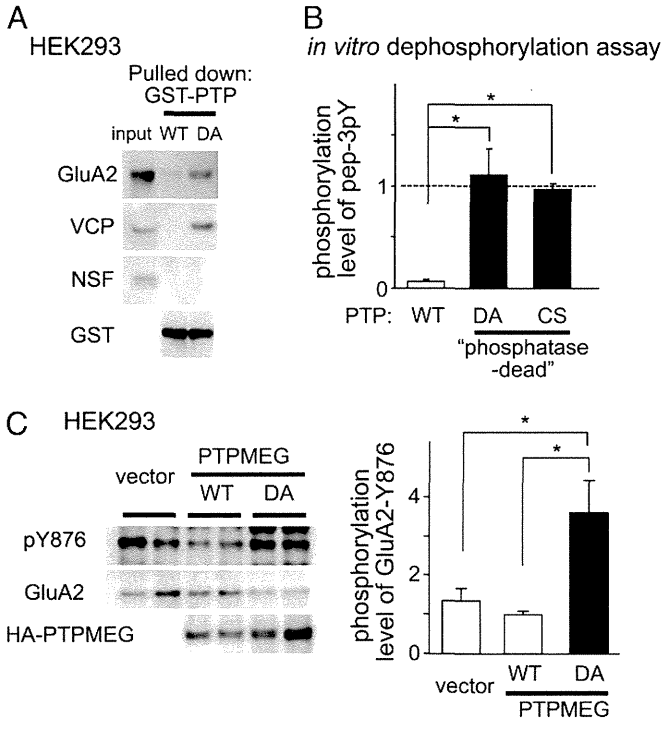

Fig. 7. GluA2 is a substrate of PTPMEG. (*A*) A substrate-trap mutant of PTPMEG interacts with GluA2. The cell lysate of HEK293 cells transfected with GluA2 was pulled down with the catalytic domain of PTPMEG fused with GST (GST-PTP). Aspartate in the catalytic center was replaced with alanine to produce a substrate-trap mutant (GST-PTP^{DA}). As reported for a related phosphatase PTPH1, endogenous VCP was trapped by GST-PTP^{DA} but not GST-PTP. *N*-ethylmaleimide–sensitive factor (NSF), a protein related to VCP, was not pulled down by GST-PTP^{DA} or GST-PTP. Similarly, GluA2 was more effectively pulled down by GST-PTP^{DA}. (*B*) GluA2 C-terminal peptides are directly dephosphorylated by PTPMEG in vitro. Cysteine in the catalytic center was replaced with serine to produce another substrate trap mutant (GST-PTP^{CS}). A tyrosine-phosphorylated synthetic peptide, pep-3pY, derived from the C terminus (869–877) of GluA2 was incubated with GST-PTP, GST-PTP^{DA}, GST-PTP^{CS}, or GST alone and subjected to the isobaric tag-based quantitative mass spectrometric analyses. The diagram indicates phosphorylation levels of peptides treated with each GST-fusion protein normalized by phosphorylation levels of peptides treated with GST alone. Bars represent mean and SEM. *$P < 0.05$ ($n = 6$ for each group). (*C*) PTPMEG dephosphorylates Y876 of GluA2 in HEK293 cells. GluA2 and WT or a phosphatase-inactive mutant (DA) PTPMEG were coexpressed in HEK293 cells, and the cell lysates were subjected to immunoblot analyses using a phosphorylation-specific antibody against pY876. Representative immunoblot images are shown in *Left*. *Right* shows intensities of pY876 bands normalized by those band intensities in cells expressing WT PTPMEG. Phosphorylation levels of Y876 of GluA2 were significantly higher in cells coexpressing a phosphatase-inactive mutant PTPMEG. The bar represents mean and SEM. *$P < 0.05$ ($n = 8$ for each group).

LTD induction in WT Purkinje cells. Conversely, the inclusion of purified Src in the patch pipette blocked LTD induction in Purkinje cells (31). Furthermore, the phosphorylation levels of Y876 in GluA2 were reduced in the synaptosomal fraction of WT cerebellar slices after chemical LTD by K-glu treatment (Fig. 2*A*). These results indicated that, similar to mGluR-dependent LTD in the hippocampus (32, 33), cerebellar LTD, which is also dependent on the mGluR, was accompanied by dephosphorylation of Y876 in GluA2.

By studying *GluD2*-null and *PTPMEG*-null cerebellum, we found unexpected interactions between the Y876 and S880 phosphorylation sites in GluA2. When basal phosphorylation levels of Y876 increased in *GluD2*-null (Fig. 1*B*) or *PTPMEG*-null (Fig. 5*B*) cerebellum, K-glu treatment failed to increase S880 phosphorylation (Figs. 2*B* and 5*D*). The application of a PP1 analog not only reduced the basal phosphorylation levels of Y876 but also restored K-glu–induced S880 phosphorylation (Fig. 2*E*) and CJ-stim–induced LTD (Fig. 3 *D–F*) in *GluD2*-null Purkinje cells. In addition, LTD was restored in *GluD2*-null Purkinje cells that expressed GluA2^{Y876F} (Fig. 3 *G–J*). Similar interactions between serine and tyrosine phosphorylation sites have been reported in other signaling molecules. For example, the serine phosphorylation of the insulin receptor substrate has been shown to hinder its tyrosine phosphorylation levels (34). The serine phosphorylation of the C terminus of the NMDA receptor subunit GluN2B also interferes with subsequent phosphorylation at a closely located tyrosine residue (35). However, in these cases, dissociation of the interacting proteins by serine phosphorylation affects local tyrosine phosphorylation. In contrast, the phosphomimetic peptide pep-3pY, which should facilitate LTD induction by competing for such interacting proteins, inhibited LTD induction in WT Purkinje cells (Fig. 4 *C* and *E*). Furthermore, an in vitro phosphorylation assay revealed that Y876 phosphorylation by Src specifically inhibited S880 phosphorylation by PKC in vitro (Fig. 2 *C* and *D*). These results indicated that S880 phosphorylation was inhibited by Y876 phosphorylation on single AMPA receptors through direct mechanisms, such as conformation changes or electrostatic charges that are associated with Y876 phosphorylation. Additional structural studies are warranted to clarify these unique interactions between the Y876 and S880 phosphorylation sites in GluA2.

The dephosphorylation of Y876 in GluA2 plays an essential role in hippocampal LTD that is induced by the mGluR agonist 3,4-dihydroxyphenylglycine (32, 33). The specific binding of BRAG2 to dephosphorylated Y876 has been shown to regulate AMPA receptor endocytosis in hippocampal neurons by activating Arf6, which turns on phosphatidylinositol 4-phosphate 5-kinase (PIP5K) to produce phosphatidylinositol (4,5)-bisphosphate and recruit adaptor protein-2 and clathrin (14). In contrast to hippocampal LTD, however, cerebellar LTD was not inhibited by the application of pep-3A (Fig. 4 *D* and *E*), which competes for BRAG2 (14). Thus, the BRAG2-Arf6 pathway may not play a major role in cerebellar LTD. Because the accumulation of adaptor protein-2 and clathrin has been shown to be required for AMPA receptor endocytosis during cerebellar LTD (9), we suspect that PIP5K may be activated by other pathways. For example, PIP5K could be activated by calcineurin in low-frequency stimulation-induced LTD in the hippocampus (36). Interestingly, PTPMEG has been shown to also be expressed in the hippocampus (15). In addition, GluD1, which is a GluD2 family member that also binds PTPMEG (Fig. S6), has been shown to be expressed in the hippocampus (37). Considering that the phosphorylation of S880 in GluA2 has been shown to be involved in hippocampal LTD under certain conditions (7, 38), we suggest that Y876 dephosphorylation could also regulate hippocampal LTD induction by direct interactions with the S880 sites in GluA2, which was observed in Purkinje cells.

Regulation of LTD by GluD2-PTPMEG Signaling. In addition to PTPMEG, other proteins, such as delphilin, bind to the C terminus of GluD2. Notably, both motor learning and LTD induction are facilitated in mice lacking delphilin (39). The FH1 domain of delphilin binds to the SH3 domain of Src in a yeast two-hybrid system (40). In addition, we found that SFK was coimmunoprecipitated with delphilin in transfected HEK293 cells (Fig. S7). Thus, although the regulation of the binding of PTPMEG and delphilin is unclear, we suggest that delphilin binding may up-regulate the phosphorylation of Y876 in GluA2 and inhibit LTD, whereas PTPMEG binding down-regulates Y876 phosphorylation and enhances LTD. Thus, Y876 phosphorylation levels, regulated by the C terminus of GluD2, may serve as a regulator of metaplasticity at PF–Purkinje cell synapses in determining LTD inducibility.

Although striatal-enriched protein tyrosine phosphatase (STEP) has been shown to play a crucial role in 3,4-dihydroxyphenylglycine–induced mGluR-dependent LTD in the hippocampus (41), it

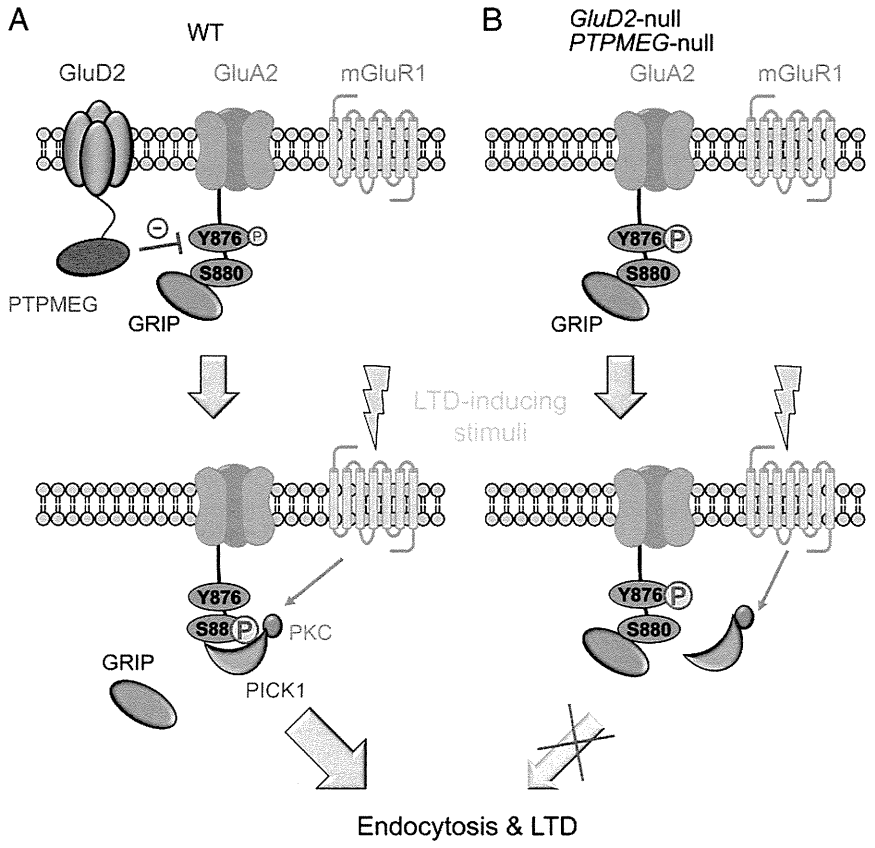

Fig. 8. A proposed role of GluD2 in the regulation of inducibility of cerebellar LTD. (*A*) In WT cerebellum, GluD2 maintains low levels of phosphorylation at Y876 of the GluA2 subunit of AMPA receptors through PTPMEG that binds to the C terminus. LTD-inducing stimuli further dephosphorylate Y876 by unknown mechanisms, including activation of PTPMEG by conformational changes of GluD2 and inactivation of SFKs. Y876 dephosphorylation allows S880 phosphorylation by PKC, leading to the replacement of anchoring proteins from glutamate receptor interacting protein (GRIP) to PICK1 and allowing AMPA receptor endocytosis during LTD. (*B*) In *GluD2*-null and *PTPMEG*-null Purkinje cells, high basal-state phosphorylation at Y876 prevents subsequent phosphorylation at S880 of GluA2 during LTD-inducing stimulus, thus inhibiting GluA2 endocytosis and LTD.

remains unclear whether Y876 in GluA2 serves as a substrate for STEP. In addition, little STEP mRNA is expressed in the cerebellum (42). In this study, we identified GluA2 as a substrate for PTPMEG with a substrate trap mutant of PTPMEG (Fig. 7*A*). An in vitro dephosphorylation assay with pep-3pY (Fig. 7*B*) and GluA2-expressing cells (Fig. 7*C*) confirmed that Y876 in GluA2 was a substrate for PTPMEG. In addition, we identified VCP as a substrate for PTPMEG with a substrate trap assay. PTPMEG has also been shown to interact with and dephosphorylate the T-cell receptor-ζ (43). Therefore, in addition to GluA2, other proteins could be dephosphorylated by PTPMEG in Purkinje cells. Because many synaptic proteins, such as β-catenin, *N*-cadherin, and ephrinB, are tyrosine-phosphorylated and regulate various aspects of synaptic functions, future studies are warranted to further identify substrates of PTPMEG.

An important question remains as to how increased neuronal activity decreases Y876 dephosphorylation (Fig. 2*A*). This dephosphorylation could be achieved independent of GluD2. For example, SFKs are down-regulated during LTD (31), thereby decreasing Y876 phosphorylation independently of GluD2. However, GluD2 may mediate not only basal but also activity-dependent Y876 dephosphorylation through the interaction with PTPMEG, because in *GluD2*-null (Fig. 2*B*) or *PTPMEG*-null (Fig. 5*D*) cerebellum, K-glu did not decrease Y876 phosphorylation. In the hippocampus, STEP is rapidly translated in response to mGluR activation (41). Because protein translation has been suggested to play a role in cerebellar LTD (44), PTPMEG may be one of the molecules with translation that is induced by mGluR. PTPMEG has also shown to be activated four- to eightfold on calpain-induced cleavage (45), which could be triggered by increases in intracellular Ca^{2+} concentrations during LTD induction. Finally, the activities of protein phosphatases have been reported to be regulated by their oligomerization status (46). Because Cbln1, which is released from granule cells, causes GluD2 clustering by binding to the N-terminal domain of GluD2 (47), it may activate PTPMEG by aggregating PTPMEG at PF synapses in Purkinje cells. D-Ser, which is released from Bergmann glia in an activity-dependent manner in immature cerebellum, binds to the ligand-binding domain of GluD2 and facilitates AMPA receptor endocytosis and LTD (48). Thus, the conformational changes that are induced by the binding of D-Ser may also regulate PTPMEG activities. Future studies are warranted to clarify whether and how GluD2-PTPMEG signaling is regulated to balance tyrosine phosphorylation and dephosphorylation levels of GluA2 for the fine tuning of AMPA receptor endocytosis.

Materials and Methods

Electrophysiology. Whole-cell patch-clamp recordings were made from visually identified Purkinje cells. Parasagittal cerebellar slices (200-μm thick) were prepared from WT, *GluD2*-null, or *PTPMEG*-null mice on P21–P35 as described previously (48). All procedures relating to the care and treatment of animals were performed in accordance with National Institutes of Health guidelines and permitted by Keio University Experimental Animal Committee.

Virus Vector Constructs and in Vivo Microinjection. For transduction of mutant transgenes into cerebellar Purkinje cells, we used a modified Sindbis virus

vector (Invitrogen), which contained an additional subgenomic promoter and GFP (3, 49). When we transduced GluA2, we used GluA2, which carried glutamine (Q) in its Q/R RNA editing site to increase cell surface expression.

Mass Spectrometric Analysis. A synthetic phosphorylated GluA2 C-terminal peptide, pep-3pY, was used as a substrate. GST-PTP^{WT}, its mutants (D820A and C852S), and GST were prebound to glutathione Sepharose beads (GE Healthcare). Dephosphorylation reaction of pep-3pY (20 pmol) was performed for 30 min at 30 °C in the buffer containing 25 mM Hepes (pH 7.35), 5 mM EDTA, and 10 mM DTT by adding 2 μg each GST protein. GluA2 peptides in the supernatant were purified and concentrated using StageTips (Empore extraction disk; 3M) and labeled with four iTRAQ reagents (Applied Biosystems/MDS Sciex). iTRAQ-labeled GluA2 peptides were mixed and concentrated by vacuum evaporation, and they were subjected to mass spectrometric analysis using a 4800 MALDI-TOF-TOF Analyzer (Applied Biosystems/MDS). Peak areas for each iTRAQ signature were obtained by using ProteinPilot. For quantitative comparison, the data were normalized by the peak area of GST-treated sample.

More details are in *SI Materials and Methods*.

Statistical Analysis. The results were described as means ± SEM. Statistical significance was defined as $P < 0.05$. When we compare the two groups, Mann–Whitney *U* test was used. We performed Student *t* test in the case of comparing the normalized values to the control (=1). To compare multiple groups, one-way ANOVA followed by Bonferroni posthoc test was performed.

ACKNOWLEDGMENTS. We thank Dr. R. L. Huganir and Dr. T. Hayashi for the antiphosphoY876 GluA2 antibody, Dr. M. Watanabe for the anti-mGluR1α antibody, and Dr. M. Mishina for the *GluD2*-null mouse. We also thank J. Motohashi and S. Narumi for their technical assistance. This work was supported by a Grant-in-Aid for the Ministry of Education, Culture, Sports, Science and Technology of Japan (to K.K., W.K., and M.Y.), the Keio Gijuku Academic Development Funds (K.K. and W.K.), the Keio University Medical Science Fund, Research Grants for Life Science and Medicine (to K.K. and W.K.), the Naito Foundation (W.K.), the Inamori Foundation (W.K.), the Nakajima Foundation (W.K.), the Takeda Science Foundation (W.K. and M.Y.), the Precursory Research for Embryonic Science and Technology (PRESTO) program from the Japan Science and Technology Agency (JST) (S.M.), and the Core Research for Evolutional Science and Technology (CREST) from the JST (M.Y.).

1. Ito M (2002) The molecular organization of cerebellar long-term depression. *Nat Rev Neurosci* 3(11):896–902.
2. Kashiwabuchi N, et al. (1995) Impairment of motor coordination, Purkinje cell synapse formation, and cerebellar long-term depression in GluR delta 2 mutant mice. *Cell* 81(2):245–252.
3. Kohda K, et al. (2007) The extreme C-terminus of GluRdelta2 is essential for induction of long-term depression in cerebellar slices. *Eur J Neurosci* 25(5):1357–1362.
4. Kakegawa W, et al. (2008) Differential regulation of synaptic plasticity and cerebellar motor learning by the C-terminal PDZ-binding motif of GluRdelta2. *J Neurosci* 28(6): 1460–1468.
5. Yuzaki M (2009) New (but old) molecules regulating synapse integrity and plasticity: Cbln1 and the delta2 glutamate receptor. *Neuroscience* 162(3):633–643.
6. Man HY, et al. (2000) Regulation of AMPA receptor-mediated synaptic transmission by clathrin-dependent receptor internalization. *Neuron* 25(3):649–662.
7. Seidenman KJ, Steinberg JP, Huganir R, Malinow R (2003) Glutamate receptor subunit 2 Serine 880 phosphorylation modulates synaptic transmission and mediates plasticity in CA1 pyramidal cells. *J Neurosci* 23(27):9220–9228.
8. Matsuda S, Launey T, Mikawa S, Hirai H (2000) Disruption of AMPA receptor GluR2 clusters following long-term depression induction in cerebellar Purkinje neurons. *EMBO J* 19(12):2765–2774.
9. Wang YT, Linden DJ (2000) Expression of cerebellar long-term depression requires postsynaptic clathrin-mediated endocytosis. *Neuron* 25(3):635–647.
10. Chung HJ, Steinberg JP, Huganir RL, Linden DJ (2003) Requirement of AMPA receptor GluR2 phosphorylation for cerebellar long-term depression. *Science* 300(5626): 1751–1755.
11. Ahmadian G, et al. (2004) Tyrosine phosphorylation of GluR2 is required for insulin-stimulated AMPA receptor endocytosis and LTD. *EMBO J* 23(5):1040–1050.
12. Moult PR, et al. (2006) Tyrosine phosphatases regulate AMPA receptor trafficking during metabotropic glutamate receptor-mediated long-term depression. *J Neurosci* 26(9):2544–2554.
13. Gladding CM, et al. (2009) Tyrosine dephosphorylation regulates AMPAR internalisation in mGluR-LTD. *Mol Cell Neurosci* 40(2):267–279.
14. Scholz R, et al. (2010) AMPA receptor signaling through BRAG2 and Arf6 critical for long-term synaptic depression. *Neuron* 66(5):768–780.
15. Hironaka K, Umemori H, Tezuka T, Mishina M, Yamamoto T (2000) The protein-tyrosine phosphatase PTPMEG interacts with glutamate receptor delta 2 and epsilon subunits. *J Biol Chem* 275(21):16167–16173.
16. Hayashi T, Huganir RL (2004) Tyrosine phosphorylation and regulation of the AMPA receptor by SRC family tyrosine kinases. *J Neurosci* 24(27):6152–6160.
17. Canepari M, Ogden D (2003) Evidence for protein tyrosine phosphatase, tyrosine kinase, and G-protein regulation of the parallel fiber metabotropic slow EPSC of rat cerebellar Purkinje neurons. *J Neurosci* 23(10):4066–4071.
18. Kim SJ, et al. (2003) Activation of the TRPC1 cation channel by metabotropic glutamate receptor mGluR1. *Nature* 426(6964):285–291.
19. Hartmann J, et al. (2008) TRPC3 channels are required for synaptic transmission and motor coordination. *Neuron* 59(3):392–398.
20. Jeromin A, Huganir RL, Linden DJ (1996) Suppression of the glutamate receptor delta 2 subunit produces a specific impairment in cerebellar long-term depression. *J Neurophysiol* 76(5):3578–3583.
21. Tanaka K, Augustine GJ (2008) A positive feedback signal transduction loop determines timing of cerebellar long-term depression. *Neuron* 59(4):608–620.
22. Huang CC, Hsu KS (2006) Sustained activation of metabotropic glutamate receptor 5 and protein tyrosine phosphatases mediate the expression of (S)-3,5-dihydroxyphenylglycine-induced long-term depression in the hippocampal CA1 region. *J Neurochem* 96(1): 179–194.
23. Yu SY, Wu DC, Liu L, Ge Y, Wang YT (2008) Role of AMPA receptor trafficking in NMDA receptor-dependent synaptic plasticity in the rat lateral amygdala. *J Neurochem* 106(2):889–899.
24. Brebner K, et al. (2005) Nucleus accumbens long-term depression and the expression of behavioral sensitization. *Science* 310(5752):1340–1343.
25. Kina S, et al. (2007) Involvement of protein-tyrosine phosphatase PTPMEG in motor learning and cerebellar long-term depression. *Eur J Neurosci* 26(8):2269–2278.
26. Tiganis T, Bennett AM (2007) Protein tyrosine phosphatase function: The substrate perspective. *Biochem J* 402(1):1–15.
27. Zhang SH, Liu J, Kobayashi R, Tonks NK (1999) Identification of the cell cycle regulator VCP (p97/CDC48) as a substrate of the band 4.1-related protein-tyrosine phosphatase PTPH1. *J Biol Chem* 274(25):17806–17812.
28. Yuzaki M, Cerebellar LTD vs. motor learning-Lessons learned from studying GluD2. *Neural Netw*, in press.
29. Boxall AR, Lancaster B, Garthwaite J (1996) Tyrosine kinase is required for long-term depression in the cerebellum. *Neuron* 16(4):805–813.
30. Hartell NA (2001) Receptors, second messengers and protein kinases required for heterosynaptic cerebellar long-term depression. *Neuropharmacology* 40(1):148–161.
31. Tsuruno S, Kawaguchi SY, Hirano T (2008) Src-family protein tyrosine kinase negatively regulates cerebellar long-term depression. *Neurosci Res* 61(3):329–332.
32. Lüscher C, Huber KM (2010) Group 1 mGluR-dependent synaptic long-term depression: Mechanisms and implications for circuitry and disease. *Neuron* 65(4):445–459.
33. Gladding CM, Fitzjohn SM, Molnár E (2009) Metabotropic glutamate receptor-mediated long-term depression: Molecular mechanisms. *Pharmacol Rev* 61(4):395–412.
34. Liu YF, et al. (2004) Serine phosphorylation proximal to its phosphotyrosine binding domain inhibits insulin receptor substrate 1 function and promotes insulin resistance. *Mol Cell Biol* 24(21):9668–9681.
35. Sanz-Clemente A, Matta JA, Isaac JT, Roche KW (2010) Casein kinase 2 regulates the NR2 subunit composition of synaptic NMDA receptors. *Neuron* 67(6):984–996.
36. Unoki T, et al. (2012) NMDA receptor-mediated PIP5K activation to produce $PI(4,5)P_2$ is essential for AMPA receptor endocytosis during LTD. *Neuron* 73(1):135–148.
37. Lomeli H, et al. (1993) The rat delta-1 and delta-2 subunits extend the excitatory amino acid receptor family. *FEBS Lett* 315(3):318–322.
38. Kim CH, Chung HJ, Lee HK, Huganir RL (2001) Interaction of the AMPA receptor subunit GluR2/3 with PDZ domains regulates hippocampal long-term depression. *Proc Natl Acad Sci USA* 98(20):11725–11730.
39. Takeuchi T, et al. (2008) Enhancement of both long-term depression induction and optokinetic response adaptation in mice lacking delphilin. *PLoS ONE* 3(5):e2297.
40. Miyagi Y, et al. (2002) Delphilin: A novel PDZ and formin homology domain-containing protein that synaptically colocalizes and interacts with glutamate receptor delta 2 subunit. *J Neurosci* 22(3):803–814.
41. Zhang Y, et al. (2008) The tyrosine phosphatase STEP mediates AMPA receptor endocytosis after metabotropic glutamate receptor stimulation. *J Neurosci* 28(42): 10561–10566.
42. Lombroso PJ, Murdoch G, Lerner M (1991) Molecular characterization of a protein-tyrosine-phosphatase enriched in striatum. *Proc Natl Acad Sci USA* 88(16):7242–7246.
43. Young JA, et al. (2008) The protein tyrosine phosphatase PTPN4/PTP-MEG1, an enzyme capable of dephosphorylating the TCR ITAMs and regulating NF-kappaB, is dispensable for T cell development and/or T cell effector functions. *Mol Immunol* 45(14):3756–3766.
44. Linden DJ (1996) A protein synthesis-dependent late phase of cerebellar long-term depression. *Neuron* 17(3):483–490.
45. Gu M, Majerus PW (1996) The properties of the protein tyrosine phosphatase PTPMEG. *J Biol Chem* 271(44):27751–27759.
46. Coles CH, et al. (2011) Proteoglycan-specific molecular switch for RPTPσ clustering and neuronal extension. *Science* 332(6028):484–488.
47. Matsuda K, et al. (2010) Cbln1 is a ligand for an orphan glutamate receptor delta2, a bidirectional synapse organizer. *Science* 328(5976):363–368.
48. Kakegawa W, et al. (2011) D-serine regulates cerebellar LTD and motor coordination through the δ2 glutamate receptor. *Nat Neurosci* 14(5):603–611.
49. Kakegawa W, Kohda K, Yuzaki M (2007) The delta2 'ionotropic' glutamate receptor functions as a non-ionotropic receptor to control cerebellar synaptic plasticity. *J Physiol* 584(Pt 1):89–96.

Satake et al. BMC Cell Biology 2013, 14:12
http://www.biomedcentral.com/1471-2121/14/12

BMC Cell Biology

RESEARCH ARTICLE Open Access

The interaction of Kinesin-1 with its adaptor protein JIP1 can be regulated via proteins binding to the JIP1-PTB domain

Tomoko Satake[1,2], Karin Otsuki[1], Yumi Banba[1], Jun Suenaga[1], Hisashi Hirano[3], Yuko Yamanaka[3], Shigeo Ohno[1] and Syu-ichi Hirai[1,4*]

Abstract

Background: The regulatory mechanisms of motor protein-dependent intracellular transport are still not fully understood. The kinesin-1-binding protein, JIP1, can function as an adaptor protein that links kinesin-1 and other JIP1-binding "cargo" proteins. However, it is unknown whether these "cargo" proteins influence the JIP1–kinesin-1 binding.

Results: We show here that JIP1–kinesin-1 binding in Neuro2a cells was dependent on conserved amino acid residues in the JIP1-phosphotyrosine binding (PTB) domain, including F687. In addition, mutation of F687 severely affected the neurite tip localization of JIP1. Proteomic analysis revealed another kinesin-1 binding protein, JIP3, as a major JIP1 binding protein. The association between JIP1 and JIP3 was dependent on the F687 residue in JIP1, and this association induced the formation of a stable ternary complex with kinesin-1. On the other hand, the binding of JIP1 and JIP3 was independent of kinesin-1 binding. We also show that other PTB binding proteins can interrupt the formation of the ternary complex.

Conclusions: The formation of the JIP1–kinesin-1 complex depends on the protein binding-status of the JIP1 PTB domain. This may imply a regulatory mechanism of kinesin-1-dependent intracellular transport.

Keywords: Kinesin-1, JIP, Cargo adaptor, PTB domain, Transport

Background

Kinesin-1, also known as conventional kinesin, is a member of the Kinesin super family proteins (KIFs). KIFs move along microtubules (MTs) by ATP hydrolysis and are essential for the transport of a variety of cargos such as protein complexes and membranous organelles [1,2]. In neurons, kinesin-1 plays a role in axonal transport of synaptic vesicles and mitochondria [1,2]. Kinesin-1 is a heterotetramer composed of two kinesin heavy chains (KHC or KIF5) and two kinesin light chains (KLC). The KHCs contain an N-terminal motor domain and a C-terminal tail region, which is required for the interaction with KLCs. The KLCs are required for the interaction with cargo proteins. Efficient intracellular transport depends on a dynamic association-dissociation cycle of motor and cargos that may involve certain regulatory molecules [1]. Kinesin-1 often employs specific adaptor proteins to carry cargos [2]. As such, the interaction between kinesin-1 and adaptor proteins can potentially serve as a regulatory point for motor-cargo assembly. However, this potential mechanism has not been directly investigated.

JNK interacting protein (JIP) 1 binds to the KLC through its C-terminal kinesin-binding site [3]. JIP1 also binds to a variety of other proteins through its JNK binding domain (JBD) and phosphotyrosine binding (PTB) domain [4-9]. Therefore, JIP1 may function as an adaptor that physically connects JIP1-binding cargo proteins and kinesin-1 to enable the transport of specific proteins. Genetic analyses of *Drosophila* axonal transport have revealed the physiological significance of JIP1 in supporting kinesin-1-dependent intracellular

* Correspondence: hirais@wakayama-med.ac.jp
[1]Department of Molecular Biology, Yokohama City University Graduate School of Medicine, Yokohama 236-0004, Japan
[4]Department of Biology, Wakayama Medical University School of Medicine, Wakayama 641-0011, Japan
Full list of author information is available at the end of the article

vesicle transport [4,5]. The binding mode of JIP1 to potential cargo proteins has been precisely analyzed. The JBD is required for interaction with JNK [6], while the PTB domain is required for interaction with various PTB domain binding proteins, including amyloid precursor protein (APP), apolipoprotein E receptor 2 (ApoER2), p190RhoGEF, dual leucine zipper bearing kinase (DLK), and JIP3 (JSAP1) [7-11]. The PTB domain binds to proteins containing an NPxY motif (or NxxY, NxxF) through an interaction dependent on a conserved phenylalanine residue in the PTB domain [12]. The corresponding phenylalanine residue of JIP1, F687, is required for interaction with the NPTY motif of APP and the NEAF motif of p190RhoGEF [8,13]. The PTB domain of JIP1 also binds to proteins which do not have typical NPxY motif including DLK and JIP3. These observations suggest a critical regulatory role for JIP1 in kinesin-1-dependent intracellular transport, and the importance of JIP1-binding proteins in regulating the formation of the JIP1–kinesin-1 complex. However, the effects of JIP1-binding proteins on the formation of the JIP1–kinesin-1 complex have not been fully determined.

In this study, we tested the significance of JIP1 binding proteins for the formation of the JIP1–kinesin-1 complex in mammalian cells. We demonstrated that conserved amino acid residues in the PTB domain, including F687, but not the JBD of JIP1 enhance the formation of a stable complex with kinesin-1, while the C-terminal residues show an absolute requirement for this interaction. We then identified another kinesin-1 binding protein, JIP3, responsible for the F687-dependent enhancement of the formation of the JIP1–kinesin-1 complex. We further analyzed the molecular basis of the enhancement of JIP1–kinesin-1 complex formation. The results not only suggest a regulatory role of JIP3 in the formation of the JIP1–kinesin-1 complex, but also suggest a possible regulatory mechanism mediated by JIP1-binding proteins that bind to the JIP1-PTB domain.

Results

Formation of the JIP1–kinesin-1 complex in Neuro2a cells is independent of the JIP1-JBD and cellular JNK activity

To examine the requirement of JIP1 binding proteins for the association between JIP1 and kinesin-1, we made a series of deletions or amino acid substitutions in the JBD and PTB domains of JIP1 (Figure 1A). The C-terminal 4 residues, which include the kinesin-1 binding site [3], were deleted in the dCT mutant, which served as a negative control. The mutated JIP1 proteins were tagged with GFP at their N termini and transiently expressed in differentiated Neuro2a cells. The association between the JIP1 mutants and kinesin-1 was estimated by an immunoprecipitation assay using anti-GFP antibody (Figure 1B and C). The results demonstrated that GFP-JIP1-WT and GFP-JIP1-dJBD showed comparable binding activity to kinesin-1, while binding activity was almost completely absent from GFP-JIP1-dCT (Figure 1B and C). Control GFP did not bind to kinesin-1. It has been reported that GFP-tagged JIP1 localizes to the neurite tips of cultured neuronal cells when the C-terminal kinesin-1 binding site is intact [3]. We confirmed the localization of GFP-JIP1 to neurite tips in a kinesin-1 binding site-dependent manner (Figure 1D, WT and dCT). This suggests that we can evaluate the association between JIP1 and kinesin-1 *in vivo* by monitoring the subcellular localization of JIP1. Thus, the localization of WT and mutant GFP-JIP1 at neurite tips was evaluated as the relative fluorescence ratio between the tips and shafts of neurites, using free GFP as a control (Figure 1E). Deletion of the N-terminal region of JIP1 that includes the JBD did not affect the localization of JIP1 to neurite tips, as expected from the binding data described above (Figure 1D, dJBD). Rather, the neurite tip localization of GFP-JIP1-dJBD was somewhat greater than GFP-JIP1-WT, although the difference was not statistically significant (Figure 1E). Because the JIP1-JBD can bind to JNK, we next tested the association between JIP1 and JNK by evaluating the co-precipitation of endogenous JNK with mutant or WT GFP-JIP1 (Additional file: 1 Figure S1A). JNK was co-precipitated with JIP1-WT, the dCT mutant and the PTB domain mutants, but not with the dJBD mutant, confirming that the dJBD mutant had lost the ability to bind JNK. Taken together, these results indicate that the JBD of JIP1 is not essential for the association between JIP1 and kinesin-1.

A possible role for JNK in the interaction between JIP1 and kinesin-1 has been proposed. In *Drosophila*, overexpression of hemipterous, an upstream kinase of the JNK ortholog, Basket, disrupts the binding of the JIP1 ortholog, APLIP1, to kinesin-1 [5]. This suggests that the binding of JIP1 to kinesin-1 depends on the activation state of JNK. However, the dJBD mutant of JIP1 that lost the ability to bind JNK apparently retained full binding activity to kinesin-1, as described above. Further, neither inhibition nor activation of JNK affected the co-precipitation of kinesin-1 with JIP1 in Neuro2a cells (Additional file: 1 Figure S1B and C). These results are consistent with the notion that JNK activity does not affect the binding of JIP1 and kinesin-1 in mammalian systems.

The PTB domain of JIP1 is required for complex formation with kinesin-1

We next examined the requirement of the PTB domain for the association between JIP1 and kinesin-1. Because deletion of the JIP1 PTB domain resulted in insoluble aggregate formation in Neuro2a cells, we used amino acid substitution to generate PTB domain mutants that lacked protein-binding activity (Figure 1A). By aligning the sequence of the JIP1 PTB domain with those of

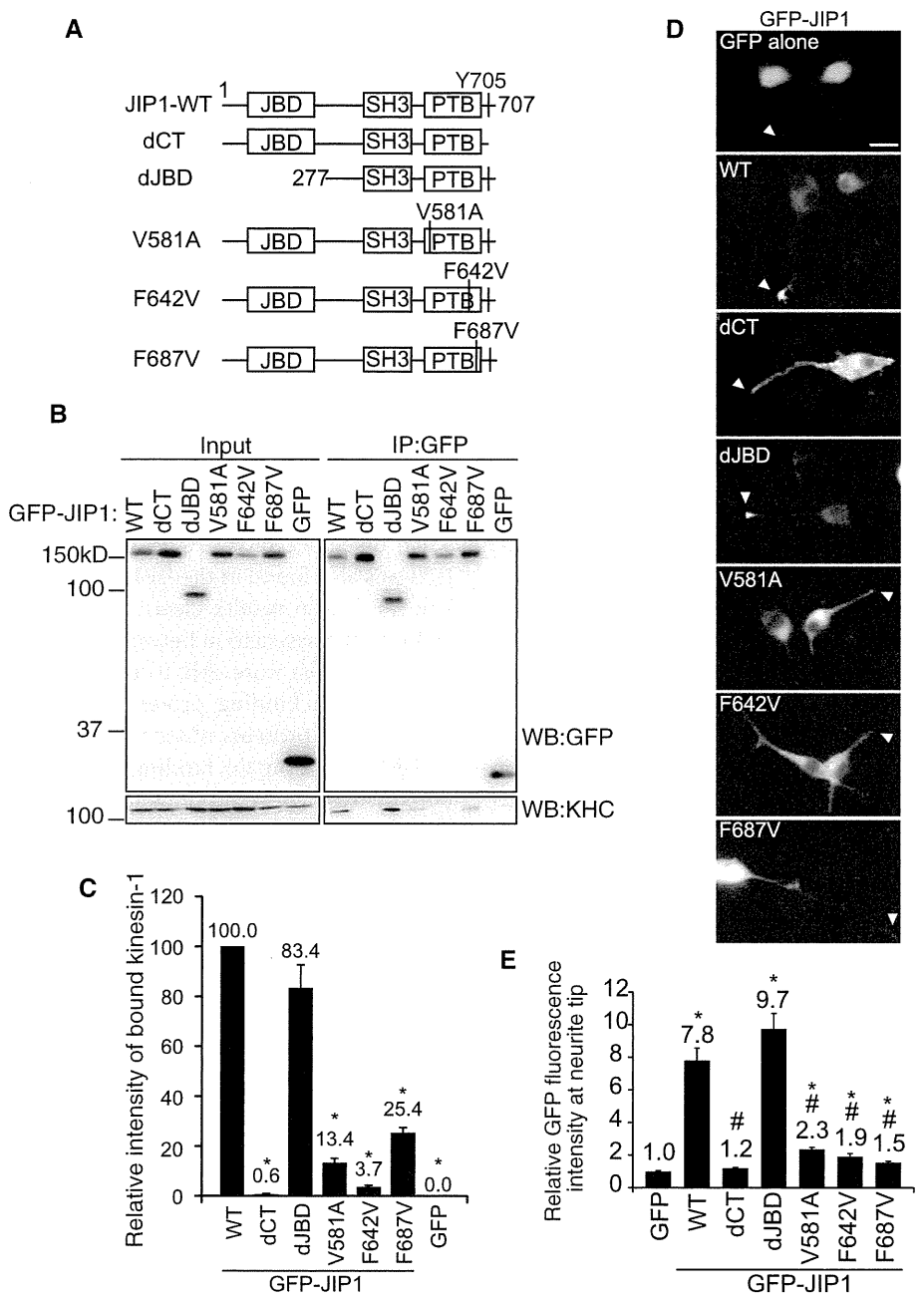

Figure 1 Formation of the JIP1–kinesin-1 complex in Neuro2a cells is dependent on the JIP1-PTB domain but not JIP1-JBD. (**A**). Schematic illustration of the JIP1 constructs used in this study. The N-terminal 276 residues were deleted in dJBD. The C-terminal 4 residues were deleted in dCT. V581, F642 and F687 were substituted by A or V in V581A, F642V and F687V. JBD: JNK binding domain; SH3: src homology 3 domain; PTB: phosphotyrosine binding domain; Y705: required tyrosine for kinesin-1 binding. These constructs are GFP- or TAP-tagged at their N-termini. (**B**). Lysates prepared from Neuro2a cells expressing GFP-JIP1 constructs or GFP alone were immunoprecipitated with anti-GFP antibody and analyzed by western blotting (WB) with the indicated antibodies. *Input*, cell lysate used for the immunoprecipitation assay. *IP:GFP*, immunoprecipitated proteins. (**C**). Quantification of kinesin-1 binding by the GFP-JIP1 constructs in (**A**). Kinesin-1 binding was normalized to the amount of precipitated GFP-JIP1. *: $p < 0.001$ compared with GFP-JIP1-WT. Error bars indicate ± SEM. $n > 3$. (**D**). Differentiated Neuro2a cells were transfected with expression vectors encoding the GFP-JIP1 constructs shown in (**A**) or GFP alone. Arrowheads indicate the neurite tips of transfected cells. Scale bar = 20 μm. (**E**). The neurite tip localization of GFP fusion proteins is shown by the relative fluorescence (tip/shaft ratio) of GFP, compensated by the value of free GFP. *: $p < 0.001$ compared with GFP. #: $p < 0.001$ compared with GFP-JIP1-WT. Error bars indicate ± SEM. $n = 117$ (GFP), 203 (WT), 183 (dCT), 213 (dJBD), 184 (V581A), 64 (F642V), 157 (F687V). These were derived from three independent experiments.

other proteins such as Dab1 and Shc, divergence between the N-terminal regions of the PTB domains in these proteins became apparent (Additional file: 2 Figure S2A). This suggests that the N-terminal region of the PTB domain is responsible for JIP1 specific functions. Alignment of JIP1 PTB domain sequences from various species revealed that V581 in this region is highly conserved (Additional file: 2 Figure S2B). Therefore, we substituted this amino acid with A to make the JIP1-V581A mutant, which was predicted to lose the ability to bind to some JIP1-specific binding proteins. Two conserved phenylalanine residues, F642 and F687, located in the C-terminal region of the JIP1 PTB domain are required for its binding to the NPTY motif of APP [13]. We replaced these F residues with V to make the JIP1-F642V and JIP1-F687V mutants, respectively (Additional file: 2 Figure S2B). We used these JIP1 mutants to examine the requirement of the PTB domain for the association between JIP1 and kinesin-1 using two independent methods described previously. As shown in Figure 1B and C, kinesin-1 binding to the GFP-JIP1-PTB domain mutants (V581A, F642V and F687V) was somewhat greater than to the dCT mutant or GFP, but far less than to GFP-JIP1-WT. The localization of GFP-JIP1 at neurite tips was also dependent on the PTB domain: none of JIP1-PTB domain mutants (V581A, F642V and F687V) showed obvious localization to the tips of neurites (Figure 1D). The neurite tip localizations of these mutants were greater than the dCT mutant or GFP, but far less than GFP-JIP1-WT (Figure 1E). Taken together, these results indicate that the PTB domain, in addition to the C-terminal region, contributes to the association between JIP1 and kinesin-1 in differentiated Neuro2a cells.

Identification of JIP3 as a principal binding protein of JIP1

The V581, F642 and F687 mutations in the PTB domain drastically reduced the binding of JIP1 to kinesin-1. Because the JIP1-PTB domain cannot directly interact with kinesin-1 [14], we hypothesized that a protein binds to the PTB domain of JIP1 and enhances the association between JIP1 and kinesin-1. We therefore searched for JIP1 binding proteins in Neuro2a cells. SDS-PAGE analysis of proteins co-precipitated with TAP-tagged JIP1 revealed a protein with an apparent molecular weight of ~180 kDa as a major binding partner of JIP1 (Figure 2A). This protein was identified as JIP3 by mass spectrometry (Additional file: 3 Figure S3). JIP3 has been reported to bind to the JIP1 PTB domain *in vitro* [11], but whether V581, F642 or F687 are required for this binding is unknown. Thus, we examined the binding between GFP-JIP1 mutants and endogenous JIP3 in Neuro2a cells by co-precipitation assays. Co-precipitation of JIP3 was observed with GFP-JIP1-WT, GFP-JIP1-dJBD and GFP-JIP1-dCT, but not with the V581A, F642V and F687V mutants or GFP (Figure 2B). These results indicate that the JIP1–JIP3 interaction in Neuro2a cells depends on V581, F642 and F687 in the JIP1 PTB domain. Accordingly, JIP3, a major JIP1-binding protein in differentiated Neuro2a cells, is a candidate protein that could enhance the association between JIP1 and kinesin-1.

To test this possibility, we performed co-precipitation assays using lysates from HEK293T cells, which did not contain detectable levels of JIP3, JIP1, and kinesin-1 proteins. Cells were transfected with expression vectors for TAP-tagged JIP1, V5-tagged KLC, and V5-tagged KHC, together with an expression vector for GFP-JIP3 or GFP. As shown in Figure 2C, the amount of kinesin-1 (V5-KLC) co-precipitated with JIP1 was significantly increased by co-expression of JIP3 (lanes 6 and 7). Because the molecular weight of V5-KHC was very close to that of TAP-tagged JIP1, we routinely detected V5-KLC when detecting TAP-JIP1 in the same gel. Notably, GFP-JIP3 was also found in the JIP1 binding fraction (Figure 2C, lane 7). These results clearly demonstrate that JIP3 can enhance the association between JIP1 and kinesin-1.

Although we were able to identify JIP3 as a major JIP1 PTB domain binding protein in differentiated Neuro2a cells, several proteins other than JIP3 have been reported as JIP1 PTB domain binding proteins in other cell systems [7-10]. These proteins include DLK and APP. DLK is a protein kinase that activates the JNK pathway [15]. DLK binding to JIP1 is mostly lost by deletion of the C-terminal part of JIP1 that includes the PTB domain [10]. APP is a vesicle-associated protein that binds to JIP1 in a manner dependent on the F642 and F687 residues of JIP1 [13]. To compare the JIP1 binding activity of these proteins, we performed co-precipitation assays using cell lysates prepared from HEK293T cells expressing GFP-fusion constructs of these JIP1 binding proteins, together with TAP-JIP1, V5-KLC and V5-KHC. Because of the low expression of full-length human APP (APP695), we used the cytoplasmic region of APP (APP-C), which contains the JIP1 binding region [7]. As shown in Figure 2C (lanes 7, 8, and 10), the amounts of GFP-DLK and GFP-APP-C in the JIP1-bound fraction were far less than GFP-JIP3, although their expression levels were rather higher (lanes 2, 3, and 5). Moreover, the expression of DLK or APP-C showed little effect on the amount of kinesin-1 co-precipitated with JIP1 (Figure 2D). These results suggest a unique function of JIP3 compared to other JIP1-binding proteins.

The association of JIP1 with JIP3 and kinesin-1 was evaluated *in vivo* by immunoprecipitation of an E17 mouse brain extract with anti-JIP1 antibody. The results clearly demonstrated that the immunoprecipitated complex containing JIP1 also contained JIP3 and kinesin-1 (Figure 2E). This result may imply the physiological significance of the association between JIP3 and JIP1.

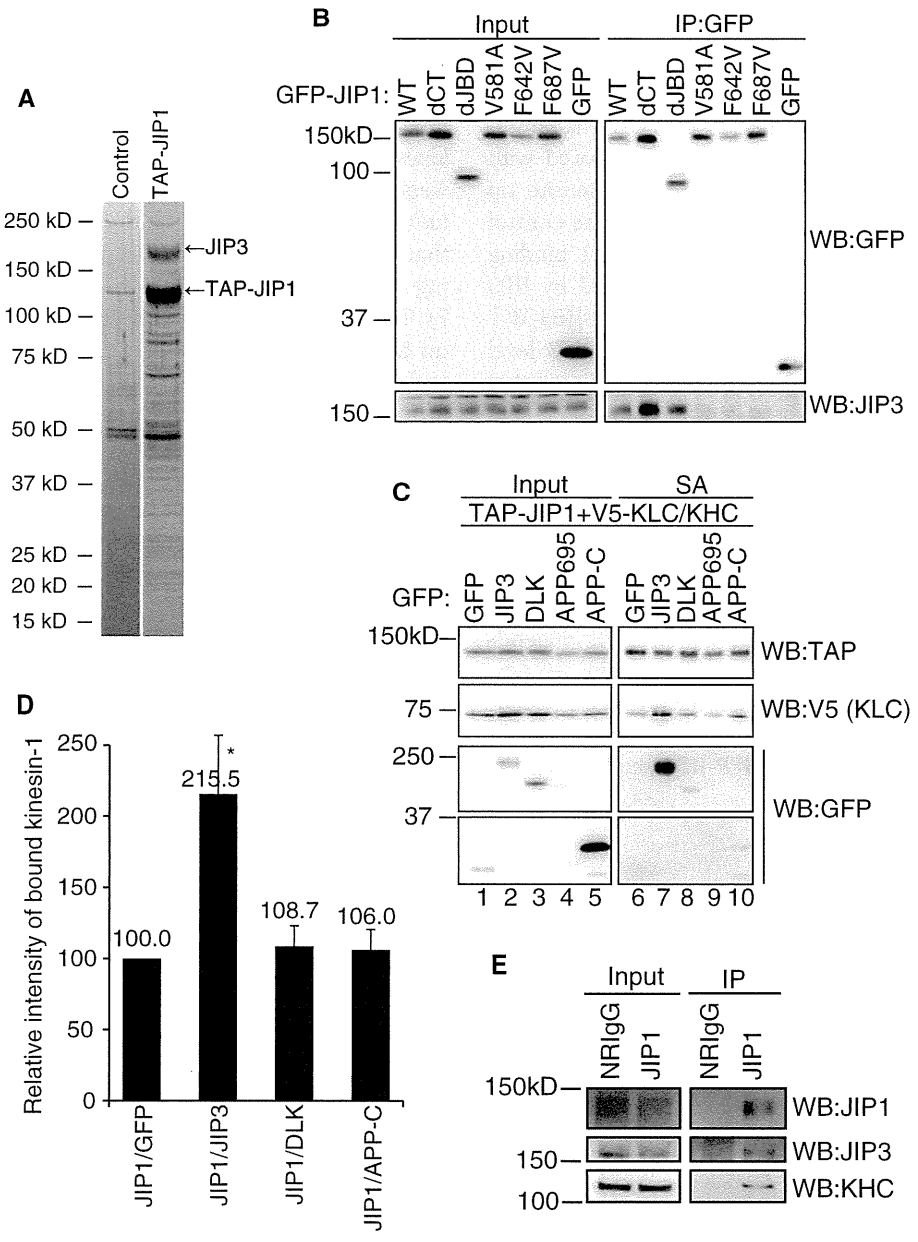

Figure 2 Identification of JIP3 as a major PTB domain-dependent binding protein of JIP1. (**A**). Neuro2a cells transiently transfected with either TAP-JIP1 or control vector were used for pull-down experiments with streptavidin sepharose (SA). The JIP1 associated polypeptides were visualized by silver staining. (**B**). Co-precipitation of GFP-JIP1 constructs and endogenous JIP3 in Neuro2a cells. The same samples as shown in Fig. 1B were analyzed by WB with the indicated antibodies. (**C**). Lysates of HEK293T cells expressing TAP-JIP1, V5-tagged kinesin light chain (V5-KLC), V5-KHC, GFP-JIP3, DLK, APP, or GFP alone were precipitated with SA and analyzed by WB with the indicated antibodies. *Input*, cell lysate used for the immunoprecipitation assay. *SA*, proteins bound to streptavidin sepharose. (**D**). Quantification of kinesin-1 (V5-KLC) binding to TAP-JIP1 in (**C**). Kinesin-1 (V5-KLC) binding was normalized to the amount of precipitated TAP-JIP1. *: $p < 0.003$ compared with GFP. Error bars indicate ± SEM. $n > 3$. (**E**). An E17 mouse brain extract was immunoprecipitated with anti-JIP1 antibody. Precipitates were analyzed by WB with the indicated antibodies.

JIP3 enhances the association between JIP1 and kinesin-1 in Neuro2a cells

To test whether JIP3–JIP1 binding is essential for the association between JIP1 and kinesin-1, we investigated the effect of JIP3 knockdown. Neuro2a cells stably expressing RFP-tagged JIP1 (RFP-JIP1-Neuro2a cells) were transiently transfected with expression vectors for JIP3 shRNA (shJIP3) or non-silencing shRNA (NS). Immunoprecipitation of RFP-JIP1 followed by western blotting using anti-KHC antibody revealed that the binding of RFP-JIP1 and kinesin-1 was severely reduced by JIP3 knockdown (Figure 3A and B). We also tested whether the JIP3 knockdown altered the

neurite tip localization of RFP-JIP1. Differentiated RFP-JIP1-Neuro2a cells were transiently transfected with shRNA vectors (NS or shJIP3) containing a GFP expression cassette to help identify the transfected cells. The localization of RFP-JIP1 to the neurite tip of GFP-labeled cells was significantly reduced in shJIP3-transfected cells compared with NS transfected cells (Figure 3C and D). The neurite tip localization of GFP was not observed in either the control cells or the JIP3-knockdown cells. The kinesin-1 binding and neurite tip localization of RFP-JIP1 reduced by JIP3 knockdown were almost recovered by the TAP-JIP3-WT expression without recovering the endogenous JIP3 level (Additional file: 4 Figure S4). These results indicate that JIP3 is crucial for the association between JIP1 and kinesin-1 in Neuro2a cells.

Molecular basis for JIP1–JIP3–kinesin-1 ternary complex formation

As shown in Figure 2C, the ectopic expression of JIP3 in HEK293T cells enhanced the association between JIP1 and kinesin-1. To confirm that the effect of JIP3 depends on the binding of JIP3 to the JIP1 PTB domain, we performed co-precipitation assays using the JIP1-F687V mutant, which showed negligible binding to JIP3 (Figure 2B). Although the expression of GFP-JIP3 enhanced the binding of TAP-tagged JIP1-WT to kinesin-1 (V5-KHC/KLC) (Figure 4A, lanes 3 and 4), the effect of JIP3 expression was negated by the JIP1 F687V mutation (Figure 4A, lanes 7 and 8). Concomitant binding of GFP-JIP3 was significantly reduced by the F687V mutation (Figure 4A, lanes 4 and 8). Nonetheless, in the absence of JIP3, the weak kinesin-1-binding activity of the JIP1-F687V mutant was comparable with that of JIP1-WT, indicating that the F687V mutation does not affect the basal binding capacity of JIP1 to kinesin-1 (Figure 4A, lanes 3 and 7). This basal kinesin-1 binding capacity was dependent on the C-terminal sequence of JIP1 (Figure 4A, lanes 3 and 11). These results indicate that JIP1–JIP3 complex formation via F687 significantly increases the kinesin-1-binding capacity of JIP1, compared with JIP1 alone.

We confirmed that roughly equal amounts of V5-KHC and V5-KLC were present in the JIP1 pull-down fraction (see Figure 4A). This suggests that V5-KHC and V5-KLC form the kinesin-1 holoenzyme in HEK293T cells and bind to JIP1.

We then sought to clarify why the JIP1–JIP3 complex showed such higher kinesin-1-binding activity. Because both JIP1 and JIP3 can bind to kinesin-1 [1], we tested whether the binding of JIP3 to kinesin-1 is essential for the stable binding of the JIP1–JIP3 complex to kinesin-1.

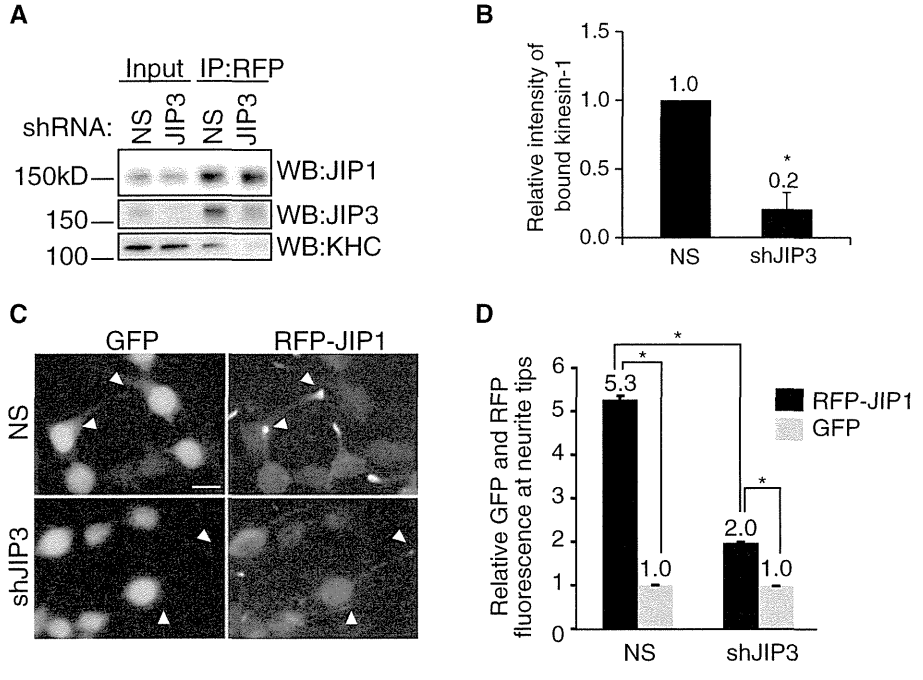

Figure 3 JIP1 requires JIP3 for binding to kinesin-1 in Neuro2a cells. (**A**). Lysates prepared from RFP-JIP1-Neuro2a cells expressing shRNA targeting JIP3 (shJIP3) or non-silencing control (NS) shRNA were immunoprecipitated with anti-RFP antibody and analyzed by WB with the indicated antibodies. *Input*, cell lysate used for the immunoprecipitation assay. IP:RFP, immunoprecipitated proteins. (**B**). Quantification of kinesin-1 binding by RFP-JIP1 in (**A**). Kinesin-1 binding was normalized to the amount of precipitated RFP-JIP1. *: $p = 0.004$ compared with NS. Error bars indicate ± SEM. n = 3. (**C**). Differentiated RFP-JIP1-Neuro2a cells were transfected with shRNA vectors (NS or shJIP3) containing a GFP expression cassette. Arrowheads indicate the neurite tips of transfected cells. Scale bar = 20 μm. (**D**). Quantification of the relative fluorescence of RFP-JIP1 and GFP in the same neurite tip. *: $p < 0.001$. Error bars indicate ± SEM. n = 200 neurites for each construct.

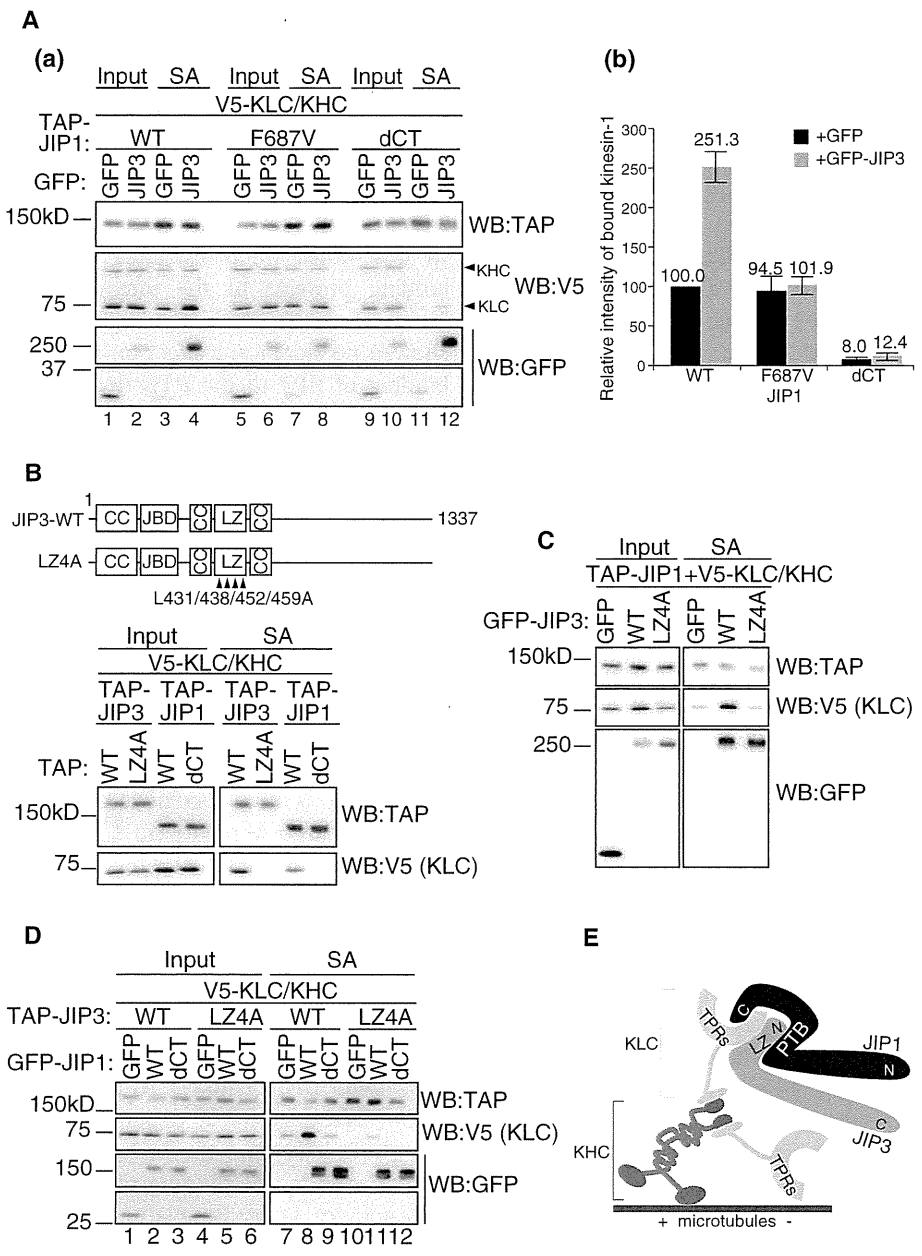

Figure 4 Molecular basis for JIP1–JIP3–kinesin-1 ternary complex formation. (**A**). Lysates prepared from HEK293T cells expressing TAP-JIP1, V5-KLC, V5-KHC and GFP-JIP3, or GFP alone, were precipitated with SA and analyzed by WB with the indicated antibodies. *Input*, cell lysate used for the immunoprecipitation assay. *SA*, proteins bound to streptavidin sepharose. Graph shows quantification of kinesin-1 (KLC) in the TAP-JIP1-bound fraction "SA". Each value was normalized to the amount of TAP-JIP1 in the corresponding SA fraction. *: $p < 0.001$ compared with TAP-JIP1-WT + GFP. Error bars indicate ± SEM. n = 3. (**B**). Upper: schematic illustration of the JIP3 constructs. The L residues (431, 438, 452 and 459) were substituted for A in the JIP3-LZ4A mutants. These constructs are GFP- or TAP-tagged at their N-termini. JBD: JNK binding domain; LZ: leucine zipper; CC: coiled-coil. Lower: lysates prepared from HEK293T cells expressing TAP-JIP3, V5-KLC and V5-KHC were precipitated with SA. TAP-JIP1 constructs were used as controls. (**C**). Lysates of HEK293T cells expressing TAP-JIP1-WT, V5-KLC, V5-KHC, GFP-JIP3 or GFP alone were precipitated with SA and analyzed by WB with the indicated antibodies. (**D**). Lysates of HEK293T cells expressing TAP-JIP3, V5-KLC, V5-KHC, GFP-JIP1 or GFP alone were precipitated with SA and analyzed by WB with the indicated antibodies. (**E**). A model of the JIP1–JIP3–kinesin-1 complex. JIP1 binds to the TPR domain of KLC via the C-terminal region. JIP3 also binds to the TPR domain of KLC via the LZ domain. Because JIP1 and JIP3 bind to distinct surfaces within the TPR domain of KLC [11], JIP3 binding to the JIP1-PTB domain can form a molecular complex that grasps the TPR domain and binds to the TPR domain more stably than JIP1 or JIP3 alone.

To disrupt the binding of JIP3 to kinesin-1, we constructed a JIP3-LZ4A mutant by substituting four L residues in the JIP3 kinesin-1 binding site, L431, L438, L452 and L459, with A (Figure 4B upper column). These L residues are conserved between JIP3 and a highly related protein, JIP4, and are directly involved in JIP4–kinesin-1 binding [16]. As shown in Figure 4B (lower column), the JIP3-LZ4A mutant failed to bind to kinesin-1. Although the JIP1-binding capacity of the JIP3-LZ4A mutant was comparable with wild-type JIP3, the ability to enhance the binding of JIP1 and kinesin-1 was completely lost in this mutant (Figure 4B, right middle panel). This result indicates that JIP3–kinesin-1 binding, as well as JIP1–kinesin-1 binding, is essential for the stable association of the JIP1–JIP3 complex with kinesin-1 (Figure 4B). This notion is confirmed by the observation that TAP-JIP3-LZ4A fails to offset the effect of JIP3 knockdown on the JIP1–kinesin-1 binding and the neurite tip localization of RFP-JIP1 (Additional file: 4 Figure S4).

Finally, we examined whether the JIP1–JIP3 complex is stabilized by kinesin-1. As shown in Figure 4A (lanes 4 and 12) and Figure 4C, disruption of the kinesin-1 binding site in both JIP1 and JIP3 did not affect the binding of JIP1 to JIP3. Moreover, concomitant disruption of JIP1 and JIP3 binding to kinesin-1 also had no effect on the binding of JIP1 to JIP3, while the binding of kinesin-1 was completely abolished (Figure 4D, lanes 8, 9, 11, and 12). These results indicate that JIP1 and JIP3 can form a stable protein complex, even in the absence of kinesin-1.

DLK affects the formation of the JIP1–JIP3–kinesin-1 ternary complex

The results presented above suggest the presence of a JIP1–JIP3–kinesin-1 ternary complex. We then tested whether the formation of the ternary complex was regulated by an additional factor, which may serve as a regulator of the JIP1–JIP3–kinesin-1 complex formation. Because the formation of the JIP1–JIP3–kinesin-1 ternary complex was highly dependent on PTB domain-dependent binding of JIP1 and JIP3, we hypothesized that other PTB domain-dependent JIP1 binding proteins would interrupt the formation of the ternary complex. If the PTB binding protein has no kinesin-1 binding activity, the binding of kinesin-1 to this protein complex will be restricted. One of the candidates for such a protein is DLK, which is reported to stably interact with JIP1 via the PTB domain, particularly when its kinase activity is suppressed [10,17]. As shown in Figure 5A and B, overexpression of a kinase-inactive mutant of DLK (DLK-KR) in Neuro2a cells did partially suppress JIP1–JIP3 binding and JIP1–kinesin-1 binding. It also suppressed the neurite tip localization of JIP1 (Figure 5C and D). A significant suppressive effect was observed only with the kinase-inactive mutant of DLK, while the effect of wild-type DLK over-expression on these binding events was not significant. This may reflect the complex regulation of the protein-binding activity of JIP1 and DLK by their phosphorylation status [17]. In any case, these results suggest a potential regulatory role for DLK in the formation of the JIP1–JIP3–kinesin-1 ternary complex.

Discussion

In this study, we investigated the contribution of JIP1 binding proteins to the interaction between JIP1 and kinesin-1. Although the binding of JNK to the JBD of JIP1 showed no significant effect on the kinesin-1 binding, the binding of JIP3 to the PTB domain of JIP1 enhanced it significantly. DLK, another JIP1-PTB domain binding protein, did not show such an effect. However, the overexpression of kinase-inactive DLK perturbed the formation of the JIP1–JIP3–kinesin-1 ternary complex, suggesting that DLK might compete with JIP3 for the JIP1-PTB domain. Taken together with the reported function of JIP1 as a cargo adaptor [3], these results suggest that the potency of the interaction between JIP1 and kinesin-1 depends on which protein binds to the JIP1-PTB domain.

JIP1 and JIP3 were originally identified as JNK binding proteins that function as a scaffold for the JNK activating protein kinase cascade in mammalian cells [18,19]. While JIP1 is now recognized as a cargo adaptor that connects cargo and kinesin-1 [3], the relationship between these distinct JIP1 functions remained unclear. It has been reported that the activation of JNK leads to the unloading of kinesin-1 from MTs [20]. However, the contribution of JIP1 or JIP3 to this process is ambiguous. A previous study in *Drosophila* suggested the possibility that JIP1–kinesin-1 binding is disrupted by JNK activation via an unidentified JNK target [5]. Because the *Drosophila* JIP1 ortholog, APLIP1, lacks the JBD, the effect of JNK may not be dependent on JIP1–JNK binding. We show here that the binding of JIP1 to kinesin-1 is not affected by the binding of JNK to JIP1, regardless of JNK activity, in mammalian cells. JIP1–JIP3 binding was also independent of JIP1–JNK binding (see Figure 2B and Additional file: 1 Figure S1A). We still cannot rule out the possibility that JIP3–JNK binding affects JIP1–JIP3 binding or JIP1–kinesin-1 binding. However, such scenarios may be unlikely because it has been reported that deletion of the JBD in JIP3 does not affect JIP3 transport in neural cells [21], and because the JIP1–JIP3 interaction in Neuro 2a cells was independent of JNK activity (see Additional file: 1 Figure S1B). Taken together, JNK seems to be a cargo of the JIP1–JIP3–kinesin-1 complex rather than a regulator of JIP1-JIP3-kinesin-1 complex formation.

In contrast to the dispensability of the JIP1 JBD, the PTB domain is essential for kinesin-1 binding by JIP1 in differentiated Neuro2a cells. We identified JIP3 as a major PTB-

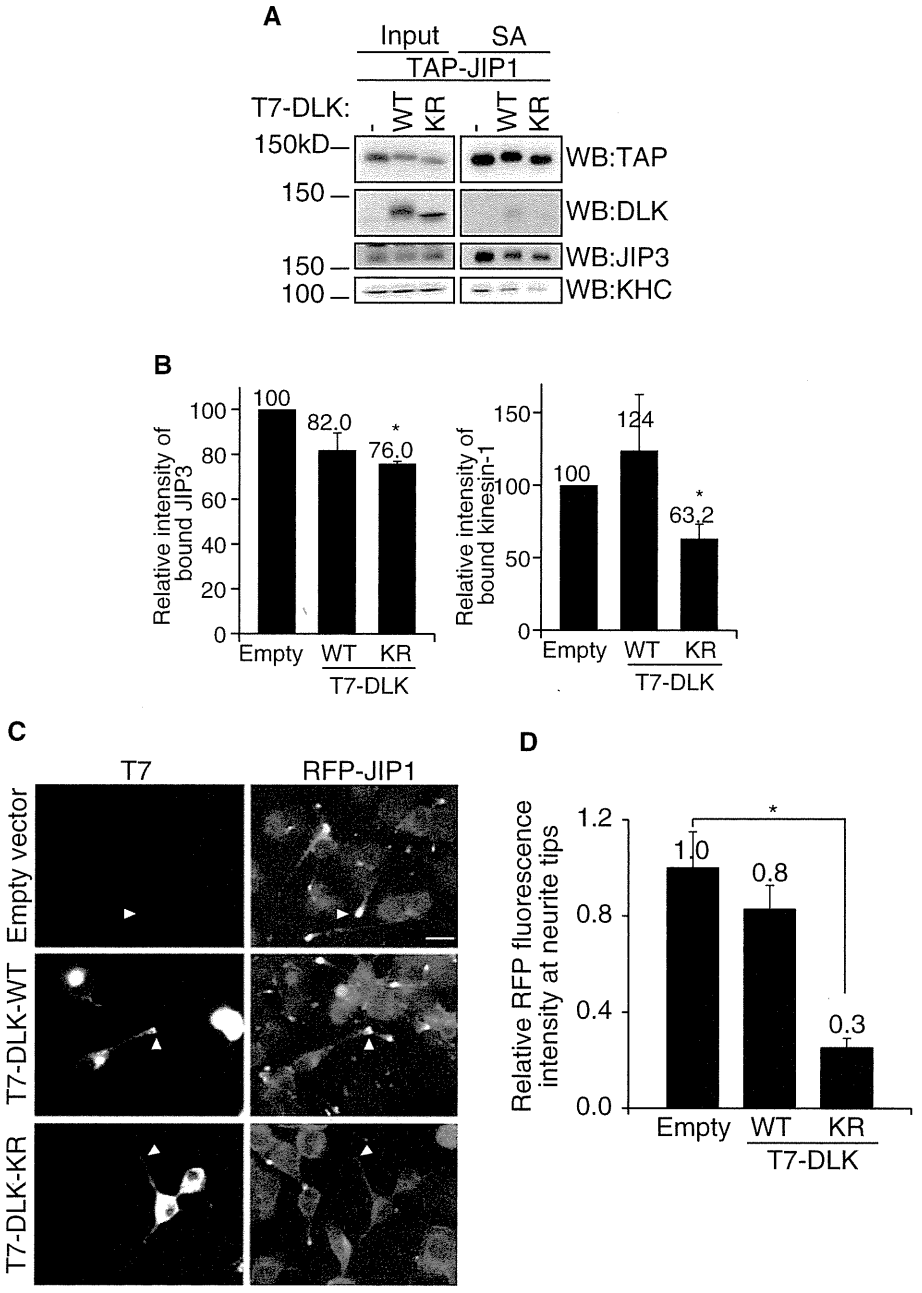

Figure 5 DLK affects the formation of the JIP1–JIP3–kinesin-1 ternary complex. (**A**). Lysates of Neuro2a cells expressing TAP-JIP1 and T7-DLK-WT, T7-DLK-KR or pUC8 were precipitated with SA and analyzed by WB with the indicated antibodies. *SA*, proteins bound to streptavidin sepharose. (**B**). Quantification of the binding of JIP3 and kinesin-1 to TAP-JIP1 in (**A**). The extent of binding was normalized to the amount of precipitated TAP-JIP1. *: $p < 0.036$ compared with Empty. Error bars indicate ± SEM. n = 4. (**C**). Differentiated RFP-JIP1-Neuro2a cells were transfected with expression vectors for T7-tagged DLK-WT, T7-DLK-KR, or pUC8 (empty vector). T7-DLK was detected by indirect immunofluorescence microscopy using anti-T7 antibody. Arrowheads indicate the neurite tips of transfected cells identified by phase contrast microscopy. Scale bar = 20 μm. (**D**). Quantification of the relative fluorescence of RFP-JIP1 at the neurite tip. *: $p < 0.001$. Error bars indicate ± SEM. n = 100 neurites for each construct.

dependent JIP1 binding protein that was largely essential for the neurite tip localization and kinesin-1-binding of JIP1. JIP1 or JIP3 bound to kinesin-1 via their kinesin-1-binding motifs, without forming a JIP1–JIP3 complex. However, this "basal" kinesin-1 binding activity was significantly enhanced by JIP1–JIP3 complex formation, which was totally dependent on the JIP1-PTB domain. A previous study showed that distinct regions of the TPR domains in KLC are responsible for JIP1 and JIP3 binding [11]. Therefore, JIP1 and JIP3 may bind to kinesin-1 in a

co-operative manner to form a stable ternary complex. This notion is further supported by the observation that the neurite tip localization of JIP1 is decreased by JIP3 knockdown (see Figure 3) [11]. It has been reported that JIP3 binds not only to kinesin light chain (KLC) but also to kinesin heavy chain (KHC) [22]. While we cannot rule out a possibility that JIP3–KHC binding contributes to the ternary complex formation, our results with a mutant JIP3 bearing amino acid substitution in the KLC contact site indicate that JIP3–KLC binding is essential for the ternary complex formation. As for JIP1–JIP3 binding, it has been reported that the central 189 amino acids of JIP3, which include the JBD and kinesin-1 binding regions, and the C-terminal 158 amino acids of JIP1, which include the PTB domain and kinesin-1 binding region, are sufficient for their binding [11]. Our results using JIP1-PTB domain point mutants further delineate the JIP3-binding domain in JIP1. By using domain specific mutants of JIP1 and JIP3, we showed that JIP1–JIP3–kinesin-1 ternary complex formation depends on JIP1–JIP3-binding, JIP1–kinesin-1-binding, and JIP3–kinesin-1-binding. Although the abrogation of one of these interactions prevented ternary complex formation, JIP1–JIP3 binding was independent of their binding to kinesin-1. This indicates that JIP1–JIP3 complex formation leads to the formation of the ternary complex. It has been reported that JIP1–kinesin-1 binding can trigger the activation of kinesin-1 motor activity in the presence of additional factors such as FEZ1 [23]. Therefore, JIP1–JIP3 complex formation might also be critical for the JIP1-dependent activation of kinesin-1.

Because the kinesin-1 binding activity of JIP3 is crucial for the formation of the ternary complex, other proteins that compete with JIP3 for binding to the JIP1-PTB domain and lack the capacity to bind kinesin-1 may negatively regulate the potency of JIP1 for kinesin-1 binding. Using DLK, we demonstrated a potential regulatory role for JIP1-PTB domain binding proteins in the formation of the JIP1–JIP3–kinesin-1 ternary complex. In addition, kinesin-1 or JIP3-binding proteins may also affect the formation of the JIP1–JIP3–kinesin-1 complex. The inhibition of JIP1–kinesin-1 binding by Ca2+–dependent binding of S100A6 to KLC, and the inhibition of JIP3–kinesin-1-binding by GTP-dependent binding of ARF6 to JIP3, have been reported [24,25]. Taken together, these observations suggest that kinesin-1-dependent transport is regulated by multiple signaling pathways via JIP1, JIP3 and KLC.

In this study, we have shown that JIP3 is a major binding protein of JIP1 in Neuro2a cells, and that JIP3 has the highest JIP1-binding capacity among various known JIP1-PTB domain binding proteins. Because JIP1 and JIP3 are highly expressed in neurons [26,27], these observations imply that JIP1 and JIP3 play a common role in kinesin-1 dependent intracellular transport. In fact, genetic studies in *Drosophila* and *Caenorhabditis elegans* have indicated that both JIP1 and JIP3 support vesicle transport in neural cells [4,28,29]. However, knockdown of JIP1 or JIP3 result in different phenotypes in mammalian neurons: JIP1 knockdown results in the partial inhibition of axon elongation, while JIP3 knockdown results in the stimulation of neurite elongation and branching [30,31]. In our experiments, although JIP3 was a major JIP1 binding protein in Neuro2a cells, only a fraction of the endogenous JIP3 was co-precipitated with endogenous JIP1 (see Figure 2E). This implies that a considerable fraction of JIP3 exists in protein complexes free of JIP1, and may have an additional function unrelated to JIP1. Therefore, the JIP1–JIP3 complex might not be a universal kinesin-1 regulatory module, but rather a specific regulator of intracellular transport in neuronal cells.

Conclusions

We investigated the contribution of JIP1 binding proteins to the interaction between JIP1 and kinesin-1. The binding of JIP3 to the PTB domain of JIP1 enhanced the JIP1–kinesin-1 interaction significantly, while the binding of JNK to the JBD of JIP1 showed no significant effect. DLK, another JIP1-PTB domain binding protein, did not show any effect on JIP1–kinesin-1 binding by itself. However, the over-expression of kinase-inactive DLK perturbed the formation of the JIP1–JIP3–kinesin-1 ternary complex, suggesting that DLK might compete with JIP3 for the JIP1-PTB domain. Our results suggest that the proteins that bind to the JIP1-PTB domain function as regulators of JIP1–kinesin-1 complex formation.

Methods

Cells

HEK293T human embryonic kidney cells, Neuro2a mouse neuroblastoma cells, and RFP-JIP1 stably transfected Neuro2a cells (RFP-JIP1-Neuro2a) were maintained in Dulbecco's modified Eagle's medium supplemented with 10% fetal bovine serum (FBS). The cell lines were cultured under 5% CO_2 at 37°C. For differentiation, Neuro2a and RFP-JIP1-Neuro2a cells were incubated with medium containing 5% FBS and 20 μM all-trans-retinoic acid (Wako) for 24–48 h.

Transfections

For transfection, 3×10^5 HEK293T or 6×10^5 Neuro2a cells were plated in 6-cm dishes. After 48 h, the cells were transfected with 5–10 μg of plasmid using Lipofectamine LTX (Invitrogen). After 24 h, the cells were used for co-precipitation assays. For knock-down of JIP3, 1×10^6 RFP-JIP1-Neuro2a cells were transfected with 3–5 μg of plasmids using either Nucleofector II (Amaxa) or Neon (Invitrogen) techniques, and plated in 6-cm dishes. After 48 h, the cells were used for co-precipitation assays. For immunofluorescence, Neuro2a and RFP-JIP1-Neuro2a cells were plated in 24-well plates for 24 h. The culture

medium was changed to differentiation medium and the cells were incubated for a further 24 h. The cells were transfected with 0.5 μg of plasmids using Lipofectamine LTX. After 24–30 h, the cells were processed for immunofluorescence staining.

Immunofluorescence and neurite tip measurements

Neuro2a and RFP-JIP1-Neuro2a cells were fixed with 3% paraformaldehyde in PBS for 15 min and washed three times with PBS. Following permeabilization with 0.1% Triton X-100 in PBS for 10 min, the cells were washed three times with PBS and quenched with 0.1 M glycine in PBS for 30 min. The cells were then washed a further three times with PBS and blocked with 10% calf serum in TBST for 1 h. All of these steps were performed at room temperature. The cells were then incubated in 0.1% BSA in TBST containing primary antibodies for 16–48 h at 4°C, washed three times with TBST, and labeled with Alexa 488-, 546-, or 647-conjugated anti-mouse or anti-rabbit antibodies. Quantification of neurite tip fluorescence intensity was performed using Multi Gauge software (Fujifilm). The neurite tip and its shaft were hand-selected with the rectangle tool, and the average pixel fluorescence intensity was measured. The average intensity ratio between the tip and shaft of individual neurites was employed as the localization value.

Co-precipitation assays

All of the following steps were performed at 4°C. The cells were washed twice with ice-cold PBS and lysed in 0.5 ml of lysis buffer (150 mM NaCl, 20 mM Hepes, pH 7.5, 1 mM EGTA, 50 mM NaF, 25 mM beta-glycerophosphate, 1 mM Na_3VO_4, pH 10, 5 μg/ml aprotinin, 10 μg/ml leupeptin, 0.5% Triton X-100, 1% protease inhibitor cocktail (Sigma)) for 10 min on ice. The lysates were then centrifuged at 15,000 × g for 20 min, and the resulting supernatants were used for co-precipitations. The supernatants were incubated with either 1 μg of antibody or Streptavidin Sepharose (GE Healthcare) for 90 min, following which the immunocomplexes were recovered with Protein A Sepharose (BD Biosciences Pharmingen). The Streptavidin Sepharose and Protein A Sepharose pellets were then washed three times with lysis buffer and boiled with SDS sample buffer.

Two whole brains from ICR E17 mouse embryos were Dounce-homogenized 10 times in 1 ml of lysis buffer and incubated on ice for 10 min. The homogenate was then centrifuged at 15,000 × g for 20 min, and the resulting supernatants were used for co-precipitations. The supernatants were incubated with either 8 μg of anti-JIP1 antibody or normal rabbit IgG for 4 hours, following which the immunocomplexes were recovered with Protein A Sepharose. The Protein A Sepharose pellets were then washed three times with lysis buffer and boiled with SDS sample buffer.

JIP1, JIP3, KLC, KHC, APP, MEKK1 and DLK expression vectors

The mouse JIP-1b cDNA (encoding a polypeptide of 707 aa) was cloned into the pEGFP-C vector (Clontech) and the pNTAP vector (Stratagene) (GFP-JIP1-WT and TAP-JIP1-WT, respectively). GFP-JIP1-WT was digested with BglII and self-ligated to generate the GFP-JIP1-dJBD vector. The GFP-JIP1-WT and TAP-JIP1-WT vectors were digested with EcoRV and ligated with a stop codon linker to generate the GFP-JIP1-dCT and TAP-JIP1-dCT vectors. As the first step in the generation of the GFP-JIP1-V581A vector, the JIP1-WT vector was digested with StuI and EcoRV, and the fragment was sub-cloned into pBlueScript KS (JIP1-PTB-pBS). Silent mutations were introduced by site-directed mutagenesis PCR to generate BsrGI and NruI sites at 571 and 590, respectively. The synthetic complementary oligonucleotides containing the V581A mutation were cloned into the BsrGI-NruI site. Then, the resultant vector was digested with BstEII and EcoRV, and the fragment was cloned into GFP-JIP1-WT. GFP-JIP1-F642V and F687V were produced by site-directed mutagenesis PCR. GFP-JIP1-V581A, -F642V and -F687V mutants were digested with BstEII and EcoRV, and the fragments were cloned into the TAP-JIP1-WT vector. Mouse JIP3-c (1337aa) was cloned into pEGFP and pNTAP vectors (GFP-JIP3-WT and TAP-JIP3-WT, respectively). GFP-JIP3-LZ4A was produced by site-directed mutagenesis PCR. GFP-JIP3-LZ4A was digested with HindIII and BglII, and the fragment was cloned into the TAP-JIP3-WT vector (TAP-JIP3-LZ4A). Mouse KLC-1d (608 aa) and KHC (KIF5C) (957 aa) were cloned into the pCMV-V5 vector (V5-KLC and V5-KHC, respectively). The T7-MEKK1, T7-DLK-WT and T7-DLK-KR vectors were described previously [15,32]. The cDNA encoding human APP (APP695) was cloned into the pEGFP-N vector. The cytoplasmic region of APP (comprising amino acids 649–695) was produced by PCR and cloned into the pEGFP-C vector (GFP-APPC).

Short hairpin RNA expression vectors

A shRNA (short hairpin RNA) plasmid targeting mouse JIP3 was constructed using DNA oligos designed with a 19-mer sense sequence, a nine-nucleotide loop, and a 19-mer antisense sequence (sense: 5′-gatccccGGTCTTG ACCCAACATGAAttcaagagaTTCATGTTGGGTCAAGA CCttttta-3′, and antisense: 5′-tcgataaaaaGGTCTTGACC CAACATGAAtctcttgaaTTCATGTTGGGTCAAGACCG GG-3′). Annealed oligos were cloned into the BglII and SalI sites of the pSuper.gfp/neo vector (OligoEngine).

Antibodies

The following antibodies were used: anti-JIP1 mAb (TDL), anti-JIP1 pAb (Zymed), anti-KHC mAb (Chemicon), anti-JIP3 pAb (Santa Cruz), anti-DLK pAb (described previously [33]), anti-JNK1 mAb (BD Biosciences Pharmingen), anti-JNK2 mAb (Santa Cruz), anti-GFP mAb (Santa Cruz), anti-GFP pAb (MBL), anti-RFP pAb (Clontech), anti-V5 mAb (Invitrogen), anti-SBP mAb for TAP-tagged proteins (Santa Cruz), anti-Omni mAb for T7-DLK (Santa Cruz), HRP-conjugated anti-rabbit IgG and anti-mouse IgG (GE Healthcare), HRP-conjugated anti-goat IgG (Zymed).

Western blotting

Proteins were separated by SDS-PAGE and analyzed by western blotting according to standard protocols. Horseradish peroxidase-conjugated secondary antibodies were used to detect bound primary antibodies. Signal intensities were quantified from the original data recorded by a LAS-4000 Multi Luminescent Image Analyzer and Multi Gauge software (Fujifilm).

Mass spectrometry analysis

Neuro2a cells (~5 × 10^7 cells) were transfected with the TAP-JIP1 expression vector. One day after transfection, retinoic acid (all-trans, Sigma) was added to the culture medium to a final concentration of 20 μM. Cells were further cultured for 2 days before lysing in 6 ml of the lysis buffer used for the co-precipitation assays (see above). The cell lysate was clarified by centrifugation at 100,000 × g for 30 min, and TAP-JIP1 binding protein was collected as described for the co-precipitation assays. The TAP-JIP1 binding proteins were separated by SDS-PAGE and detected by silver staining for imaging or by SYPRO Ruby (Molecular Probes) for mass spectrometry. The band of interest was cut out and digested with trypsin. The eluted peptides were analyzed on a 4800 MALDI TOF/TOF system (Applied Biosystems).

Additional files

Additional file 1: Figure S1. JNK activity does not affect JIP1 binding to kinesin-1. (**A**). Co-precipitation of GFP-JIP1 mutants and endogenous JNK in Neuro2a cells. The same samples as shown in Fig. 2A were analyzed by WB with the indicated antibodies. (**B**). Neuro2a cells transiently expressing TAP-JIP1 were treated with SP600125 (20 μM) or DMSO (vehicle) for 2 hours. Lysates were precipitated with SA. *SA*, proteins bound to streptavidin sepharose. (**C**). RFP-JIP1-Neuro2a cells were transfected with expression vectors for T7-MEKK1 or pUC8 (empty vector). Lysates were immunoprecipitated with anti-RFP antibody and analyzed by WB with the indicated antibodies. *: non-specific band.

Additional file 2: Figure S2. Sequence alignments of the JIP1 PTB domain. (**A**) JIP1 PTB domain aligned with Shc- and Dab1-PTB domains. All sequences are from mouse. The gray shading indicates the amino acids corresponding to JIP1 V581, F642 and F687. (**B**). Alignment of JIP1 PTB domains between species. The gray shading indicates the amino acids corresponding mouse JIP1 V581, F642 and F687.

Additional file 3: Figure S3. Mouse JIP3 peptides identified by Mascot search (Matrix Science). Amino acid sequence of mouse JIP3. Capital letters shaded gray indicate the peptides identified by Mascot search.

Additional file 4: Figure S4. The effect of JIP3 knockdown was offset by JIP3-WT but not JIP3-LZ4A. (**A**). Lysates prepared from RFP-JIP1-Neuro2a cells expressing shRNA targeting JIP3 (shJIP3), non-silencing control (NS) shRNA, TAP-JIP3-WT, or TAP-JIP3-LZ4A, in the combination as indicated were immunoprecipitated with anti-RFP antibody and analyzed by WB with the indicated antibodies. Input, cell lysate used for the immunoprecipitation assay. IP:RFP, immunoprecipitated proteins. (**B**). Quantification of kinesin-1 binding by RFP-JIP1 in (A). Kinesin-1 binding was normalized to the amount of precipitated RFP-JIP1 and input of kinesin-1. Results of two independent experiments are shown. (**C**). Differentiated RFP-JIP1-Neuro2a cells were transfected with shRNA vectors (NS or shJIP3) containing a GFP expression cassette. Arrowheads indicate the neurite tips of transfected cells. Scale bar = 20 μm. (**D**). Quantification of the relative fluorescence of RFP-JIP1 in the neurite tip. *: $p < 0.03$. Error bars indicate ± SEM. n = 50 for each construct.

Abbreviations

JIP: c-Jun N-terminal kinase (JNK) interacting protein; PTB: Phosphotyrosine binding; KHC: Kinesin heavy chain; KLC: Kinesin light chain; APP: Amyloid precursor protein; DLK: Dual leucine zipper bearing kinase; WT: Wild type.

Competing interests

The authors declare that they have no competing interests.

Authors' contributions

TS and SH designed the experiments. TS and KO performed and analyzed the immunoprecipitation assays. TS performed and analyzed the immunofluorescence assays. HH and YY performed the mass spectrometry analysis. TS, KO, YB, JS and SH constructed the expression vectors. TS, SH and SO wrote the manuscript. All authors read and approved the final manuscript.

Acknowledgements

We thank Dr. T.C. Saido for kindly providing the human APP cDNA, and Dr. I. Nishimoto for the mouse JIP1 cDNA. This work was supported by JSPS KAKENHI Grant Number 21570184.

Author details

[1]Department of Molecular Biology, Yokohama City University Graduate School of Medicine, Yokohama 236-0004, Japan. [2]Molecular Medicine and Informatics Doctoral Program, Yokohama City University Graduate School of Medicine, Yokohama 236-0004, Japan. [3]Department of Supramolecular Biology, International Graduate School of Arts and Sciences, Yokohama City University, Yokohama 230-0045, Japan. [4]Department of Biology, Wakayama Medical University School of Medicine, Wakayama 641-0011, Japan.

Received: 12 October 2012 Accepted: 6 February 2013
Published: 4 March 2013

References

1. Hirokawa N, Noda Y: **Intracellular transport and kinesin superfamily proteins, KIFs: structure, function, and dynamics.** *Physiol Rev* 2008, **88**:1089–1118.
2. Hirokawa N, Noda Y, Tanaka Y, Niwa S: **Kinesin superfamily motor proteins and intracellular transport.** *Nat Rev Mol Cell Biol* 2009, **10**:682–696.
3. Verhey KJ, Meyer D, Deehan R, Blenis J, Schnapp BJ, Rapoport TA, Margolis B: **Cargo of kinesin identified as JIP scaffolding proteins and associated signaling molecules.** *J Cell Biol* 2001, **152**:959–970.
4. Horiuchi D, Barkus RV, Pilling AD, Gassman A, Saxton WM: **APLIP1, a kinesin binding JIP-1/JNK scaffold protein, influences the axonal transport of both vesicles and mitochondria in Drosophila.** *Curr Biol* 2005, **15**:2137–2141.
5. Horiuchi D, Collins CA, Bhat P, Barkus RV, Diantonio A, Saxton WM: **Control of a kinesin-cargo linkage mechanism by JNK pathway kinases.** *Curr Biol* 2007, **17**:1313–1317.

6. Dickens M, Rogers JS, Cavanagh J, Raitano A, Xia Z, Halpern JR, Greenberg ME, Sawyers CL, Davis RJ: **A cytoplasmic inhibitor of the JNK signal transduction pathway.** *Science* 1997, **277**:693–696.
7. Scheinfeld MH, Roncarati R, Vito P, Lopez PA, Abdallah M, D'Adamio L: **Jun NH2-terminal kinase (JNK) interacting protein 1 (JIP1) binds the cytoplasmic domain of the Alzheimer's beta-amyloid precursor protein (APP).** *J Biol Chem* 2002, **277**:3767–3775.
8. Meyer D, Liu A, Margolis B: **Interaction of c-Jun amino-terminal kinase interacting protein-1 with p190 rhoGEF and its localization in differentiated neurons.** *J Biol Chem* 1999, **274**:35113–35118.
9. Stockinger W, Brandes C, Fasching D, Hermann M, Gotthardt M, Herz J, Schneider WJ, Nimpf J: **The reelin receptor ApoER2 recruits JNK-interacting proteins-1 and −2.** *J Biol Chem* 2000, **275**:25625–25632.
10. Ikeda A, Hasegawa K, Masaki M, Moriguchi T, Nishida E, Kozutsumi Y, Oka S, Kawasaki T: **Mixed lineage kinase LZK forms a functional signaling complex with JIP-1, a scaffold protein of the c-Jun NH(2)-terminal kinase pathway.** *J Biochem* 2001, **130**:773–781.
11. Hammond JW, Griffin K, Jih GT, Stuckey J, Verhey KJ: **Co-operative versus independent transport of different cargoes by Kinesin-1.** *Traffic* 2008, **9**:725–741.
12. Uhlik MT, Temple B, Bencharit S, Kimple AJ, Siderovski DP, Johnson GL: **Structural and evolutionary division of phosphotyrosine binding (PTB) domains.** *J Mol Biol* 2005, **345**:1–20.
13. Taru H, Kirino Y, Suzuki T: **Differential roles of JIP scaffold proteins in the modulation of amyloid precursor protein metabolism.** *J Biol Chem* 2002, **277**:27567–27574.
14. Matsuda S, Matsuda Y, D'Adamio L: **Amyloid beta protein precursor (AbetaPP), but not AbetaPP-like protein 2, is bridged to the kinesin light chain by the scaffold protein JNK-interacting protein 1.** *J Biol Chem* 2003, **278**:38601–38606.
15. Hirai S, Izawa M, Osada S, Spyrou G, Ohno S: **Activation of the JNK pathway by distantly related protein kinases. MEKK and MUK.** *Oncogene* 1996, **12**:641–650.
16. Nguyen Q, Lee CM, Le A, Reddy EP: **JLP associates with kinesin light chain 1 through a novel leucine zipper-like domain.** *J Biol Chem* 2005, **280**:30185–30191.
17. Nihalani D, Wong HN, Holzman LB: **Recruitment of JNK to JIP1 and JNK-dependent JIP1 phosphorylation regulates JNK module dynamics and activation.** *J Biol Chem* 2003, **278**:28694–28702.
18. Whitmarsh AJ, Cavanagh J, Tournier C, Yasuda J, Davis RJ: **A mammalian scaffold complex that selectively mediates MAP kinase activation.** *Science* 1998, **281**:1671–1674.
19. Ito M, Yoshioka K, Akechi M, Yamashita S, Takamatsu N, Sugiyama K, Hibi M, Nakabeppu Y, Shiba T, Yamamoto KI: **JSAP1, a novel jun N-terminal protein kinase (JNK)-binding protein that functions as a Scaffold factor in the JNK signaling pathway.** *Mol Cell Biol* 1999, **19**:7539–7548.
20. Stagi M, Gorlovoy P, Larionov S, Takahashi K, Neumann H: **Unloading kinesin transported cargoes from the tubulin track via the inflammatory c-Jun N-terminal kinase pathway.** *FASEB J* 2006, **20**:2573–2575.
21. Sato S, Ito M, Ito T, Yoshioka K: **Scaffold protein JSAP1 is transported to growth cones of neurites independent of JNK signaling pathways in PC12h cells.** *Gene* 2004, **329**:51–60.
22. Sun F, Zhu C, Dixit R, Cavalli V: **Sunday Driver/JIP3 binds kinesin heavy chain directly and enhances its motility.** *EMBO J* 2011, **30**:3416–3429.
23. Blasius TL, Cai D, Jih GT, Toret CP, Verhey KJ: **Two binding partners cooperate to activate the molecular motor Kinesin-1.** *J Cell Biol* 2007, **176**:11–17.
24. Shimamoto S, Takata M, Tokuda M, Oohira F, Tokumitsu H, Kobayashi R: **Interactions of S100A2 and S100A6 with the tetratricopeptide repeat proteins, Hsp90/Hsp70-organizing protein and kinesin light chain.** *J Biol Chem* 2008, **283**:28246–28258.
25. Montagnac G, Sibarita JB, Loubery S, Daviet L, Romao M, Raposo G, Chavrier P: **ARF6 Interacts with JIP4 to control a motor switch mechanism regulating endosome traffic in cytokinesis.** *Curr Biol* 2009, **19**:184–195.
26. Akechi M, Ito M, Uemura K, Takamatsu N, Yamashita S, Uchiyama K, Yoshioka K, Shiba T: **Expression of JNK cascade scaffold protein JSAP1 in the mouse nervous system.** *Neurosci Res* 2001, **39**:391–400.
27. Pellet JB, Haefliger JA, Staple JK, Widmann C, Welker E, Hirling H, Bonny C, Nicod P, Catsicas S, Waeber G, *et al*: **Spatial, temporal and subcellular localization of islet-brain 1 (IB1), a homologue of JIP-1, in mouse brain.** *Eur J Neurosci* 2000, **12**:621–632.
28. Bowman AB, Kamal A, Ritchings BW, Philp AV, McGrail M, Gindhart JG, Goldstein LS: **Kinesin-dependent axonal transport is mediated by the sunday driver (SYD) protein.** *Cell* 2000, **103**:583–594.
29. Byrd DT, Kawasaki M, Walcoff M, Hisamoto N, Matsumoto K, Jin Y: **UNC-16, a JNK-signaling scaffold protein, regulates vesicle transport in C. elegans.** *Neuron* 2001, **32**:787–800.
30. Dajas-Bailador F, Jones EV, Whitmarsh AJ: **The JIP1 scaffold protein regulates axonal development in cortical neurons.** *Curr Biol* 2008, **18**:221–226.
31. Suzuki A, Arikawa C, Kuwahara Y, Itoh K, Watanabe M, Watanabe H, Suzuki T, Funakoshi Y, Hasegawa H, Kanaho Y: **The scaffold protein JIP3 functions as a downstream effector of the small GTPase ARF6 to regulate neurite morphogenesis of cortical neurons.** *FEBS Lett* 2010, **584**:2801–2806.
32. Hirai S, Kawaguchi A, Hirasawa R, Baba M, Ohnishi T, Ohno S: **MAPK-upstream protein kinase (MUK) regulates the radial migration of immature neurons in telencephalon of mouse embryo.** *Development* 2002, **129**:4483–4495.
33. Hirai S, Cui de F, Miyata T, Ogawa M, Kiyonari H, Suda Y, Aizawa S, Banba Y, Ohno S: **The c-Jun N-terminal kinase activator dual leucine zipper kinase regulates axon growth and neuronal migration in the developing cerebral cortex.** *J Neurosci* 2006, **26**:11992–12002.

doi:10.1186/1471-2121-14-12
Cite this article as: Satake *et al.*: The interaction of Kinesin-1 with its adaptor protein JIP1 can be regulated via proteins binding to the JIP1-PTB domain. *BMC Cell Biology* 2013 **14**:12.

JOURNAL OF PROTEOMICS 84 (2013) 40–51

Available online at www.sciencedirect.com

SciVerse ScienceDirect

www.elsevier.com/locate/jprot

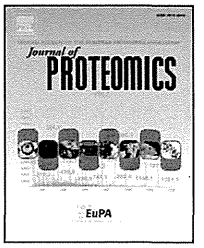

Differential proteome analysis of serum proteins associated with the development of type 2 diabetes mellitus in the KK-A^y mouse model using the iTRAQ technique

Eri Takahashi[a,b,1], *Akinori Okumura*[a,1], *Hiroyuki Unoki-Kubota*[a,1], *Hisashi Hirano*[b], *Masato Kasuga*[c], *Yasushi Kaburagi*[a,*]

[a]*Department of Diabetic Complications, Diabetes Research Center, Research Institute, National Center for Global Health and Medicine, Tokyo, Japan*
[b]*Graduate School of Nanobioscience, Yokohama City University, Yokohama, Japan*
[c]*National Center for Global Health and Medicine, Tokyo, Japan*

ARTICLE INFO

Article history:
Received 24 October 2012
Accepted 19 March 2013

Keywords:
Serum proteome
Type 2 diabetes mellitus
Quantitative mass spectrometry
Multiple reaction monitoring

ABSTRACT

To identify candidate serum molecules associated with the progression of type 2 diabetes mellitus (T2DM), we carried out differential proteomic analysis using the KK-A^y mouse, an animal model of T2DM with obesity. We employed an iTRAQ-based quantitative proteomic approach to analyze the proteomic changes in the sera collected from a pair of 4-week-old KK-A^y versus C57BL/6 mice. Among the 227 proteins identified, a total of 45 proteins were differentially expressed in KK-A^y versus C57BL/6 mice. We comparatively analyzed a series of the sera collected at 4 and 12 weeks of age from KK-A^y and C57BL/6 mice for the target protein using multiple reaction monitoring analysis, and identified 8 differentially expressed proteins between the sera of these mice at both time points. Among them, serine (or cysteine) peptidase inhibitor, clade A, member 3K (SERPINA3K) levels were elevated significantly in the sera of KK-A^y mice compared to C57BL/6 mice. An *in vitro* assay revealed that the human homologue SERPINA3 increased the transendothelial permeability of retinal microvascular endothelial cells, which may be involved in the pathogenesis of diabetes and/or diabetic retinopathy. With the identified proteins, our proteomics study could provide valuable clues for a better understanding of the underlying mechanisms associated with T2DM.

Biological significance

In this paper, we investigated the serum proteome of KK-A^y mice in a pre-diabetic state compared to that of wild type controls in an attempt to uncover early diagnostic markers of diabetes that are maintained through a diabetic phenotype. We used iTRAQ-based two-dimensional LC–MS/MS serum profiling, and identified several differentially expressed proteins at the pre-diabetic stage. The differential expression was confirmed by multiple reaction monitoring assay, which is fast gaining ground as a sensitive, specific, and cost-effective methodology for relative quantification of the candidate proteins. Using these techniques, we have identified eight candidate proteins of interest including SERPINA3K, which may be important in the pathology of T2DM and/or diabetic retinopathy.

* *Corresponding author at:* Department of Diabetic Complications, Diabetes Research Center, Research Institute, National Center for Global Health and Medicine, 1-21-1 Toyama, Shinjuku-ku, Tokyo 162-8655, Japan. Tel.: +81 3 3202 7181x2931; fax: +81 3 3202 7364.
E-mail address: kaburagi@ri.ncgm.go.jp (Y. Kaburagi).
[1] Contributed equally.

1874-3919/$ – see front matter © 2013 Elsevier B.V. All rights reserved.
http://dx.doi.org/10.1016/j.jprot.2013.03.014

1. Introduction

Diabetes mellitus is one of the most common metabolic disorders in the world, in which more than 90% of patients are diagnosed with type 2 diabetes mellitus (T2DM) [1]. The pathogenesis of T2DM is thought to be complicated, involving multiple genetic, metabolic, and environmental factors. Typically, it is characterized by hyperglycemia that is caused by defects in insulin secretion and its molecular action [2]. Initially, the effect of T2DM is limited to the detrimental loss of insulin-producing pancreatic β-cells. However, subsequent reduction in insulin secretion may lead to multiple malfunctions such as macrovascular complications including cardiovascular and cerebrovascular diseases, and microvascular complications including diabetic retinopathy and nephropathy [3].

Identifying individuals at high risk of T2DM prior to the clinical onset of the multiple malfunctions associated with T2DM is a major goal in diabetes research. Therefore, many efforts have been made to identify genetic and protein markers to reveal the molecular/cellular details or progression of diabetes [4–9]. Genome wide association studies have some clear advantages because genetic susceptibility, which does not change over time, can be identified at an early stage. While these markers provide a good foundation for the prediction and prevention of T2DM, the available tests are far from satisfactory due to their low-to-moderate sensitivity/specificity and/or late appearance in the disease process. As such, markers with increased specificity/sensitivity are urgently needed.

Proteomics has been used to identify novel disease markers that are differentially expressed during a pathological state in patients compared to healthy individuals. The systemic nature of T2DM indicates that the modulation of plasma proteins may be the cause or a consequence of the pathophysiology of this disease. To date, a few proteomic analyses of plasma related to T2DM have been reported [10–12]; however, analysis of the plasma proteomics of T2DM has been very limited and requires further investigations to find reliable diagnostic marker protein. Further, most previous serum proteomic analyses of T2DM have focused on the discovery of biomarkers, and have not stressed their potential to elucidate the pathophysiological mechanisms of the disease. Thus, the potential of serum proteomics to investigate the underlying disease mechanisms has been poorly addressed.

In this study, we analyzed the KK-A^y mouse model of T2DM in a pre-diabetic state. KK-A^y mice are obese, develop severe early-onset hyperinsulinemia, hyperglycemia, hypertriglyceridemia, and fatty liver, and are widely used as a model for T2DM [13]. We applied iTRAQ labeling coupled with offline 2-D LC–MS/MS proteomics technology to analyze quantitatively the protein expression profile of KK-A^y and C57BL/6 mice as well as to identify novel diagnostic marker proteins associated with the pathophysiological mechanisms of T2DM. To verify the candidate proteins that were differentially expressed among the two groups in the iTRAQ discovery study, we analyzed the time course changes of the candidate protein levels in the sera of KK-A^y and C57BL/6 mice using multiple reaction monitoring (MRM) analysis. We identified 8 proteins, including serine proteinase inhibitor A3K (SERPINA3K), that were expressed between the 2 groups. We further revealed that the human homologue SERPINA3 increased the permeability of retinal microvascular endothelial cells, which may be involved in the pathogenesis of diabetes and/or diabetic retinopathy.

2. Materials and methods

2.1. Mouse sample collection

KK-A^y/TaJcl (KK-A^y) and C57BL/6JJcl (C57BL/6) mice were purchased from Clea Japan Inc. (Tokyo, Japan). The mice were housed individually and fed standard mouse chow and water. At 4, 8, 12 and 16 weeks of age, body weights and fasting blood glucose levels were measured as described previously (n = 4/each group) [14]. Oral glucose tolerance test (OGTT) was performed on conscious mice after a 16 h fasting (n = 4/each group). The test was done by orally administrated glucose (2 mg per g body weight) and measurement of blood glucose at 15, 30, 45 and 60 min after loading. To perform proteomic analysis associated with the early onset of T2DM, we studied 4- and 12-week-old KK-A^y and C57BL/6 mice as a reference. Blood samples were obtained from retro-orbital venous plexus of the mice which had fasted over 16 h. The serum was immediately separated by centrifugation at 3000×*g* for 20 min at 4 °C, and was stored at −80 °C until analyzed. Animal care, use, and experimental protocols were approved by the local animal ethics committee of the National Center for Global Health and Medicine (approval ID: 12034) and performed in accordance with EU Directive 2010/63/EU.

2.2. Protein depletion and purification

For each group (C57BL/6 mice at 4 weeks, KK-A^y mice at 4 weeks, C57BL/6 mice at 12 weeks, and KK-A^y mice at 12 weeks), serum samples were prepared from the male mice. The seven most abundant proteins (albumin, IgG, α1-antitrypsin, IgM, transferrin, haptoglobin and fibrinogen) were depleted by using Seppro Mouse Spin Columns following the manufacturer's protocol (Sigma-Aldrich, St. Louis, MO, USA). The collected samples were desalted and concentrated using Amicon Ultra-4 3K (Millipore, Billerica, MA, USA). Protein concentration was determined using the Bradford protein assay (Bio-Rad Protein Assay; Bio-Rad Laboratories, Hercules, CA, USA).

2.3. iTRAQ labeling

An equal amount of depleted samples from each group was digested with MS-grade Trypsin Gold (Promega, Madison, WI, USA) and the peptides were labeled with iTRAQ reagents according to the manufacturer's instructions (iTRAQ Reagents 4-plex Applications Kit; AB Sciex, Framingham, MA, USA). Briefly, 25 μg of each depleted sample was reduced with 50 mM tris-(2-carboxyethyl)phosphine, alkylated with 84 mM iodoacetamide, and digested with Trypsin Gold at a protein-to-enzyme ratio of 10:1 at 37 °C overnight. For the analysis of serum protein expression in the KK-A^y mice, the tryptic digest samples prepared from the 3 KK-A^y mice were labeled with iTRAQ reagents (iTRAQ reporter ions of 115.1, 116.1 and 117.1 *m/z*). An equal amount of samples from the 3 KK-A^y mice and 3 C57BL/6 mice was pooled, labeled with

iTRAQ reporter ions of 114.1 *m/z*, and used as an internal standard (Supplementary Fig. 1). The sample set consisting of the 3 KK-A^y mice samples and an internal standard were combined and dried using a centrifugal concentrator (TOMY SEIKO CO., LTD., Tokyo, Japan) and dissolved in 100 μL of 10 mM ammonium formate, 25% ACN and 0.5% formic acid. For the analysis of serum protein expression in the C57BL/6 mice, the tryptic digest samples prepared from the 3 C57BL/6 mice were labeled with iTRAQ reagents (iTRAQ reporter ions of 115.1, 116.1 and 117.1 *m/z*). The sample set consisting of the 3 C57BL/6 mice samples and an internal standard were combined, dried, and dissolved in 10 mM ammonium formate, 25% ACN and 0.5% formic acid as well.

2.4. *Separation with strong cation exchange chromatography (SCX)*

Two iTRAQ labeled sample sets were fractionated separately using HPLC (Gilson Medical, Middleton, WI, USA) equipped with a model 305 LC pump, a UV/VIS-155detector, Rheodyne injection valve (model 7725) with 500 μL fixed loop injector, an FC203B autosampler, and a TSK gel SP-2SW column (4.6 mm I.D. × 250 mm cm, ϕ5 μm; TOSOH, Tokyo, Japan) (Supplementary Fig. 1). The mobile phase consisted of (A); 10 mM ammonium formate and 25% ACN, pH 3.0 and (B); 500 mM ammonium formate and 25% ACN, pH 6.8. The mixed iTRAQ labeled samples were dissolved in 100 μL of buffer A and separated at a flow rate of 0.6 mL/min using a 2-step liner gradient; 0% B for 10 min, 0–30% B for 40 min, 30%–100% for 10 min, and 100% B for 10 min. A total of 18 fractions were collected, dried using the centrifugal concentrator, dissolved in 2% ACN and 0.1% TFA, and desalted with MonoSpin C18 (GL Science, Tokyo, Japan).

2.5. *NanoLC–MS/MS*

Fractionated samples prepared from each iTRAQ labeled sample set were analyzed by LC–MS/MS (Supplementary Fig. 1). NanoLC–MS/MS system was conducted by a QSTAR ELITE Q-TOF mass spectrometry (AB Sciex) equipped with a nano-electro-spray ionization source, a nanoLC system (Paradigm MS4; Michrom Bioresources, Auburn, CA, USA), and an HTC-PAL autosampler (CTC Analytics, Zwingen, Switzerland). The SCX-fractionated peptides dissolved in 2% ACN and 0.1% TFA were loaded onto a trap column (0.3 × 5 mm, L-Column ODS; Chemicals Evaluation and Research Institute, Tokyo, Japan), and separated by RP capillary LC (L-Column Micro; Chemicals Evaluation and Research Institute) at a flow rate of 300 nL/min. The eluent gradient consisted of 95% buffer A (2% ACN and 0.1% TFA) to 45% buffer B (90% ACN and 0.1% TFA) for 120 min. A spray voltage of 1800 V was applied.

2.6. *Data analysis of iTRAQ experiments*

Peptide and protein identification was performed through automated database searching using the Mascot search engine (version 2.4.0; Matrix Science, London, UK). All tandem mass spectra were searched for species of *Mus musculus* against the UniProtKB/Swiss-Prot database containing 536,489 sequence entries (release—2012_06). Carbamidomethylation of cysteine and iTRAQ reagents (N-terminus and Lysine side chain) were chosen as the fixed modifications, and oxidation of methionine and iTRAQ reagents (Tyrosine) were searched as the variable modifications. Searches were performed with trypsin cleavage specificity allowing 1 missed cleavage; mass tolerance for monoisotopic peptide identification was set to ±0.1 Da and ±0.1 Da for fragment ions. The instrument setting was "ESI-QUAD-TOF". For the relative quantification of each peptide, the ratio of the areas under the signature peaks of 115, 116, 117, and 114 Da (as an internal standard), which are the masses of the tags that correspond to the iTRAQ reagents, was used. Data file processing and relative quantification were performed using ProteinPilot 3.0 software (AB Sciex) and the Paragon algorithm. The search parameters used were: iTRAQ 4-plex (peptide labeled), carbamidomethylation of cysteine, and UniProtKB/Swiss-Prot database for *M. musculus*. The confidence threshold for protein identification was an unused ProtScore >1.3 (95% confidence interval). Protein quantification required at least one unique peptide, and relative protein quantitation value normalized to an internal standard for each sample was used for the statistical analysis.

2.7. *Protein networks and functional analysis*

Differentially expressed serum proteins between the KK-A^y and C57BL/6 mice were subjected to functional pathway analysis using Ingenuity Pathway Analysis (IPA) (Ingenuity Systems, available at www.ingenuity.com). Protein analysis was performed through Database for Annotation, Visualization and Integrated Discovery (DAVID) version 6.7 (available at http://david.abcc.ncifcrf.gov/home.jsp) [15].

2.8. *Multiple reaction monitoring (MRM) analysis*

For making transitions for each peptide in MRM, MRMPilot software version 2.0 (AB Sciex) was used. High-confidence peptides with a rich product ion spectrum for each target protein were selected for relative quantification analysis using MRM. Peptides that had modifications, such as partially oxidized methionine, were avoided and when possible, two peptides were used per protein. MRM run was performed using a 5500 QTRAP hybrid triple quadrupole/linear ion trap mass spectrometer (AB Sciex) coupled with a Paradigm MS4 nanoLC system in the MRM mode. Test runs of the synthetic peptides mixture were performed to establish the retention time window (±5 min) for each peptide ion. During the test run, full scan MS/MS acquisitions (EPI, Enhanced Product Ion) were also triggered when MRM signal exceeded 1000 counts, with a mass tolerance of 250 mDa, the Linear Ion Trap (LIT) was set at 5 ms fixed fill time. Samples were separated on a C18 column (L-Column Micro, L-Column ODS; Chemicals Evaluation and Research Institute) with solvent A (2% ACN and 0.1% formic acid) and solvent B (90% ACN and 0.1% formic acid). The flow rate was set to 300 nL/min at room temperature, after which linear gradient elution was performed by increasing the mobile phase composition from 5 to 40% solvent B over 90 min. The gradient was then ramped to 95% B for 10 min and 5% B for 10 min to equilibrate the column for the next run. The total LC running time was 110 min. A 5500 QTRAP mass spectrometer was interfaced with a nanospray

source. The ionspray voltage was set to 2300 V. The source temperature was set to 150 °C. The curtain gas, collision gas, and ion source gas 1 were 10, 12, and 15, respectively. The declustering potential, entrance potential, and collision cell exit potential were set to 70 V, 10 V, and 15 V, respectively. Unit resolutions were used at quadrupole part 1 and quadrupole part 3. The collision energy for each transition was calculated by MRMPilot software version 2.0. In the MRM runs, the target scan time was set to 2 s. Five hundred ng of mouse serum sample was digested with mass spectrometry grade Trypsin Gold and Lysyl Endopeptidase (Wako Pure Chemicals, Osaka, Japan) for MRM analysis. The digested sample was transferred to a new tube and 10 fmol of human CUB domain containing protein 1 peptide (EEGVFTVTPDTK) was also added to each sample as an internal standard. Samples were analyzed by LC–MRM on the 5500 QTRAP using the predetermined MRM method. Data were processed using the MultiQuant program (version 2.0; AB Sciex). The most intense peak of the transition was used for quantitation. The area under the most intense peak was calculated, and normalized to the input internal standard. The peak of the transition for the input internal standard was also used for the quality control measure. Duplicate analyses were performed for each of the mouse serum samples.

2.9. *Cell culture*

Primary human retinal microvascular endothelial cells (HRMVECs) were purchased from the Applied Cell Biology Research Institute (Kirkland, WA, USA). HRMVECs were cultured on type I collagen-coated cell culture dishes in EGM-2 MV medium (EBM-2 supplemented with EGM-2 MV SingleQuots; Lonza, Walkersville, MD, USA). The cells were used at passages 7–9.

2.10. *Expression and purification of recombinant human SERPINA3 protein*

Human *SERPINA3* cDNA excluding signal sequences was amplified from human liver mRNA (Clontech, Palo Alto, CA, USA) by RT-PCR and cloned into the expression vector pET-21a(+) (Merck KGaA, Darmstadt, Germany). The C-terminal histidine-tagged SERPINA3 protein was expressed in *Escherichia coli* BL21 (DE3) cells and purified by Ni-NTA affinity chromatography, as described previously [16]. The protein was passed through a polymyxin B affinity column (Detoxi-gel Endotoxin Removing Columns; Thermo Scientific, Rockford, IL, USA) to remove contaminating endotoxins. The eluted SERPINA3 protein was concentrated with a membrane filter (Amicon Ultra-15 3K; Millipore) and stored at −80 °C until use.

2.11. *Electric cell substrate impedance sensing (ECIS) assays*

Transendothelial electrical impedance was measured using an ECIS Zθ instrument (Applied Biophysics, Troy, NY, USA). HRMVECs were plated at confluence in 8W10E+ (for barrier functional measurement) or 8W1E (for wound-healing assay) gold electrode culture plates (Applied Biophysics) precoated with type I collagen. The cells were cultured in EGM-2 MV medium for 16 h, after which the medium was changed to EBM-2 medium supplemented with 0.5% FBS (Lonza). For barrier functional measurement, HRMVECs were incubated with SERPINA3 protein at a final concentration ranging from 100 to 500 μg/mL and the incubation was continued for a further 40 h. Multi-frequency measurements (11 frequencies at 0.0625, 0.125, 0.25, 0.5, 1, 2, 4, 8, 16, 32, and 64 kHz) were taken for each of the 16 wells at a fixed interval of 180 s. To better characterize the divergent changes in barrier function caused by SERPINA3 in HRMVECs, we applied the model of Giaever and Keese [17] to resolve our ECIS data into three components: Rb (cell-to-cell resistances), α (cell-to-extracellular matrix interaction), and Cm (membrane capacitance). For the wound-healing assays, serum-starved confluent cells treated with SERPINA3 at a final concentration ranging from 100 to 500 μg/mL for 6 h were submitted to an elevated voltage pulse of 60 kHz frequency, 1400 μA amplitude, and 20 s duration, which killed and removed cells from the electrode. The kinetics of wound closure over the electrode were then assessed by continuous impedance measurements at 16 kHz for 24 h. HRMVECs incubated without SERPINA3 were used as a control.

2.12. *Cell proliferation analysis by 5-bromo-2′-deoxyuridine (BrdU) incorporation*

HRMVECs (1.0×10^4 cells/well) were seeded in type I collagen-coated 96 well plates with EGM2 MV medium for 16 h and incubated with EBM2 medium supplemented with 0.5% FBS for another 8 h. The cells were treated with SERPINA3 protein for 18 h, after which BrdU labeling solution was added and incubated for another 6 h. The proliferation rate was measured using cell proliferation ELISA, BrdU chemiluminescence kit (Roche Applied Science, Mannheim, Germany) according to the manufacturer's protocol.

2.13. *Data analysis and statistics*

The distributions of continuous data were tested for normality by the Shapiro–Wilk test. Values were presented as mean ± SD for normally distributed values. Differences between the groups were tested using Student's two-sided *t*-test or a two-tailed Mann–Whitney *U* test, as appropriate. All calculations were performed with Microsoft Excel 2010 or the SPSS software version 20 (IBM, Armonk, NY, USA). The differences were considered statistically significant for p values smaller than 0.05.

3. Results

3.1. *Comparative analysis of the serum proteomic changes in the paired KK-A^y versus C57BL/6 mice*

Characteristics of KK-A^y mice are shown in Fig. 1. KK-A^y mice were originally developed by Nishimura by crossing the KK mouse with the A^y mouse (C57BL/6J-A^y) [18]. C57BL/6J mice are generally used as nondiabetic controls. Therefore, we used C57BL/6J mice as a control for KK-A^y. As KK-A^y mice grew older, body weight and glucose concentration were gradually increased as reported previously [14]. Body weights of KK-A^y mice were significantly increased from 4 to 16 weeks of age